

A mutation in LXR α uncovers a role for cholesterol sensing in limiting metabolic dysfunction-associated steatohepatitis

Received: 25 May 2024

Accepted: 17 January 2025


Published online: 28 January 2025

Alexis T. Clark^{1,3}, Lillian Russo-Savage^{1,2,3}, Luke A. Ashton¹, Niki Haghsheenas¹, Nicolas A. Amselle¹ & Ira G. Schulman¹ 

Liver x receptor alpha (LXR α) functions as an intracellular cholesterol sensor that regulates lipid metabolism at the transcriptional level in response to the direct binding of cholesterol derivatives. We have generated mice with a mutation in LXR α that reduces activity in response to endogenous cholesterol derived LXR ligands while still allowing transcriptional activation by synthetic agonists. The mutant LXR α functions as a dominant negative that shuts down cholesterol sensing. When fed a high fat, high cholesterol diet LXR α mutant mice rapidly develop pathologies associated with Metabolic Dysfunction-Associated Steatohepatitis (MASH) including ballooning hepatocytes, liver inflammation, and fibrosis. Strikingly LXR α mutant mice have decreased liver triglycerides but increased liver cholesterol. Therefore, elevated cholesterol in the liver may play a critical role in the development of MASH. Reengaging LXR signaling by treatment with synthetic agonist reverses MASH in LXR α mutant mice suggesting that LXR α normally functions to impede the development of liver disease.

Metabolic Dysfunction-Associated Steatotic Liver Disease (MASLD, formally referred to as non-alcoholic fatty liver disease) is estimated to impact ~25% of the adult population in the United States and 35% of adults worldwide¹. MASLD by itself can be relatively benign but ~25% of patients progress to Metabolic Dysfunction-Associated Steatohepatitis (MASH, formally referred to as non-alcoholic steatohepatitis), characterized by hepatocyte ballooning, inflammation of the liver, and fibrosis. Importantly, MASH increases the risk for cirrhosis, hepatocellular carcinoma, and liver failure². The processes triggering the progression of MASLD to MASH or even if there is a true stepwise progression from one pathological state to the other, however, remains to be determined. MASLD is characterized by excess fat accumulation in the liver and elevated rates of de novo fatty acid synthesis are often observed^{3,4}. Since most MASLD patients do not have MASH, it is not clear if increases in liver fat alone drive the transition to MASH or if additional triggers are required.

In humans, liver cholesterol levels correlate with the severity of MASH^{5–8} and clinical studies indicate that patients with MASH can benefit from inhibiting cholesterol synthesis with statins^{9–13}. Furthermore, most high-fat diet-dependent rodent models of MASH also require high levels of dietary cholesterol to promote disease^{14–17}. High intracellular cholesterol is toxic leading to endoplasmic reticulum stress, inflammation, and cell death all of which have been suggested to contribute to MASH². Nevertheless, the mechanisms by which cholesterol directly influences the disease are not well established. The liver X receptors, LXR α (Nr1h3) and LXR β (Nr1h2), are members of the nuclear hormone receptor superfamily of ligand-activated transcription factors that function as important regulators of cholesterol and fatty acid metabolism. By directly binding cholesterol derivatives including oxidized forms of cholesterol (oxysterols) LXRs sense changes in intracellular cholesterol levels and regulate gene expression to maintain lipid homeostasis^{18–20}. Like many nuclear receptors, in

¹Department of Pharmacology, University of Virginia School of Medicine, Charlottesville, VA, USA. ²Present address: Department of Neurological Sciences, University of Vermont, Burlington, VT, USA. ³These authors contributed equally: Alexis T. Clark, Lillian Russo-Savage.  e-mail: igs4c@virginia.edu

the absence of agonist ligands LXRs can interact with corepressor proteins that inhibit transcription. Binding of either endogenous or synthetic agonists results in conformational changes in the LXR ligand binding domain that reduce interaction with corepressors and favor engagement with coactivators that increase transcription of LXR-regulated genes²¹. Genetic deletion of LXR α , the major LXR subtype expressed in the liver, impairs the catabolism and excretion of cholesterol and also decreases de novo fatty acid synthesis^{22,23}. Consistent with the genetic data, molecular studies indicate that LXRs directly regulate the transcription of genes involved in cholesterol excretion, the synthesis of bile acids from cholesterol, and fatty acid synthesis^{22,24–26}. Since elevated fatty acid synthesis is considered a major driver of steatosis in MASLD, inhibiting LXR activity has been put forward as a potential therapeutic approach for treating steatotic liver disease²⁷. Indeed, treatment with synthetic LXR antagonists reduces hepatic lipid accumulation in diet-dependent mouse models of liver steatosis^{28–30}. On the other hand, increasing LXR activity in mice with synthetic agonists promotes cholesterol excretion from the liver, the net movement of cholesterol out of the body, and reduces inflammation^{23,31,32}. Accordingly, even in the face of large increases in hepatic and plasma triglyceride levels, LXR activation has beneficial effects in models of chronic metabolic diseases including type II diabetes and atherosclerosis^{33–36}. In support of the mouse models, genome-wide association studies in humans have identified variants in the human LXR α gene (*NRIH3*) linked to lipid levels and insulin sensitivity^{37–39}. Rare variants in LXR α are also associated with markers of liver damage⁴⁰ suggesting an important role for LXR α in maintaining normal liver function.

We have generated mice with mutation of a conserved tryptophan at amino acid position 441 of the LXR α gene to phenylalanine (W441F). The W441F mutation impairs the transcriptional response of LXR α to endogenous cholesterol-derived ligands while still allowing transcriptional regulation with potent synthetic agonists^{41–43}. LXR α W441F functions as a dominant negative receptor that inhibits LXR-dependent transcription in vivo. Mutant mice accumulate cholesterol in the liver and demonstrate increased pro-inflammatory and pro-fibrotic gene expression. In response to a high-fat, high-cholesterol diet W441F mice rapidly develop MASH-like phenotypes including ballooning hepatocytes, immune infiltration, and fibrosis. Reengaging LXR signaling by treating W441F mice with synthetic LXR agonists reverses cholesterol accumulation, inflammation, and fibrosis suggesting that LXRs normally function to impede the development of MASH.

Results

Characterization of LXR α W441F

Structural studies and reporter gene assays suggest that mutation of a conserved tryptophan in the carboxy-terminal helix 12 of the LXR ligand binding domain (amino acid 441 in mouse LXR α) to phenylalanine weakens pi-cation interactions with a histidine in helix 10 (amino acid 419 in mouse LXR α) that is required for the transcriptional response of LXRs to cholesterol derived ligands. Transcriptional activation by potent synthetic ligands such as T0901317 that directly hydrogen bond with histidine 419, however, is less sensitive to the change to phenylalanine^{41–43}. To explore the effect of the W441F mutation in a more relevant setting, immortalized bone marrow-derived macrophages derived from LXR α +LXR β double knockout mice⁴⁴ were infected with adenovirus expressing mouse LXR α or LXR α W441F and the mRNAs encoding sterol regulatory element binding protein 1c (*Srebp1c*) and stearoyl CoA desaturase 1 (*Scd1*), two well-characterized LXR target genes, were quantified. Cells infected with virus expressing GFP alone were used as controls (Fig. 1a, b). As expected, wildtype LXR α increases gene expression in response to both the oxysterol 24(s),25-epoxycholesterol as well as the synthetic agonist T0901317. In contrast, the response to

24(s),25-epoxycholesterol is selectively lost in cells expressing LXR α W441F. Dose-response analysis indicates that the EC₅₀ for T0901317 is increased by a factor of 5 in cells expressing LXR α W441F and that the maximum efficacy is reduced relative to cells expressing wildtype LXR α (Fig. 1c). Synthetic agonists that do not form hydrogen bonds with histidine 419 such as GW3965 and BMS852927^{45–47} demonstrate little or no ability to activate LXR α W441F (Supplemental Fig. 1). Western blotting indicates that the mutant protein is expressed at higher levels than the wildtype LXR α (Fig. 1d, e) which is consistent with our published studies demonstrating that LXR half-life correlates with transcriptional activity⁴⁸.

To examine the consequence of the W441F mutation in vivo, CRISPR was used to introduce the mutation into the *Lxra* (*Nr1h3*) locus (Supplemental Fig. 2a). Breeding of heterozygous mutant mice (referred to as W/F) produces homozygous wildtype (referred to as W/W) and homozygous mutant (referred to as F/F) progeny at the expected mendelian ratios. At 10–12 weeks of age there are no significant differences in body weight among W/W, W/F, and F/F females or males (Supplemental Fig. 2b) and all mice appear normal. LXR-regulated genes involved in cholesterol metabolism (Fig. 2a–c) and fatty acid synthesis (Fig. 2d–f), however, are significantly decreased in the livers and intestines of W441F mice compared to controls with relatively stronger decreases in homozygous (F/F) compared to heterozygous (W/F) mutant animals. Western blotting demonstrates approximately equal levels of LXR α protein in liver nuclear extracts from each of the 3 genotypes (Supplemental Fig. 2d, e) indicating the observed changes in gene expression do not result from decreased W441F protein levels. There is a corresponding decrease in plasma triglycerides and cholesterol (Fig. 2g, h) which reflects known roles for LXRs in promoting very low density lipoprotein (VLDL) secretion^{26,49,50} and the production of high-density lipoprotein particles^{31,51,52}. Plasma glucose is slightly lower in mutant mice (Fig. 2i), however, the decrease in glucose may be secondary to liver damage (see below). Consistent with the known role for LXR α in regulating bile acid synthesis²², fecal bile acids are also decreased in W441F mice (Supplemental Fig. 2c). Since LXR α W441F is not activated by endogenous cholesterol-derived ligands, we suggest that mutant receptors function as dominant negative inhibitors of transcription by binding to DNA but failing to activate transcription. Indeed, overexpressing LXR α W441F in AML12 mouse liver cells inhibits expression of LXR target genes (Supplemental Fig. 2f–h).

Histological examination of liver sections by hematoxylin and eosin (H&E) staining uncovers evidence of immune infiltration in homozygous F/F W441F mice (Fig. 3a). Additionally large pockets of neutral lipids are selectively detected by Oil Red staining of homozygous F/F mutant sections (Fig. 3b). Quantification of tissue lipids indicates that liver triglycerides are decreased in both heterozygous W/F and homozygous F/F mice (Fig. 3c).

Liver cholesterol on the other hand is increased only in homozygous F/F mutant mice (Fig. 3d, e) suggesting that the Oil Red O staining most likely identifies cholesterol-loaded cells. The observation that LXR target genes involved in cholesterol catabolism are less affected in heterozygous mutants relative to genes involved in fatty acid synthesis (Fig. 2a–f) may account for the gene dosage effects on hepatic cholesterol accumulation. Hepatomegaly, evidenced by larger liver-to-body weight ratios, is also observed selectively in F/F mice (Supplemental Fig. 3a). Furthermore, increased staining with antibodies recognizing the proliferative marker Ki67 is detected in F/F hepatocyte nuclei (Fig. 3f) indicating cell division is occurring. Previous studies have suggested that transcriptionally active LXRs constrain cell growth by limiting the availability of cholesterol needed to support proliferation^{53–55}. The increase in hepatocyte proliferation measured in homozygous F/F mutant mice supports the earlier work and further indicates that LXR signaling normally limits hepatocyte growth. Finally, the levels of alanine transaminase (ALT), and aspartate amino

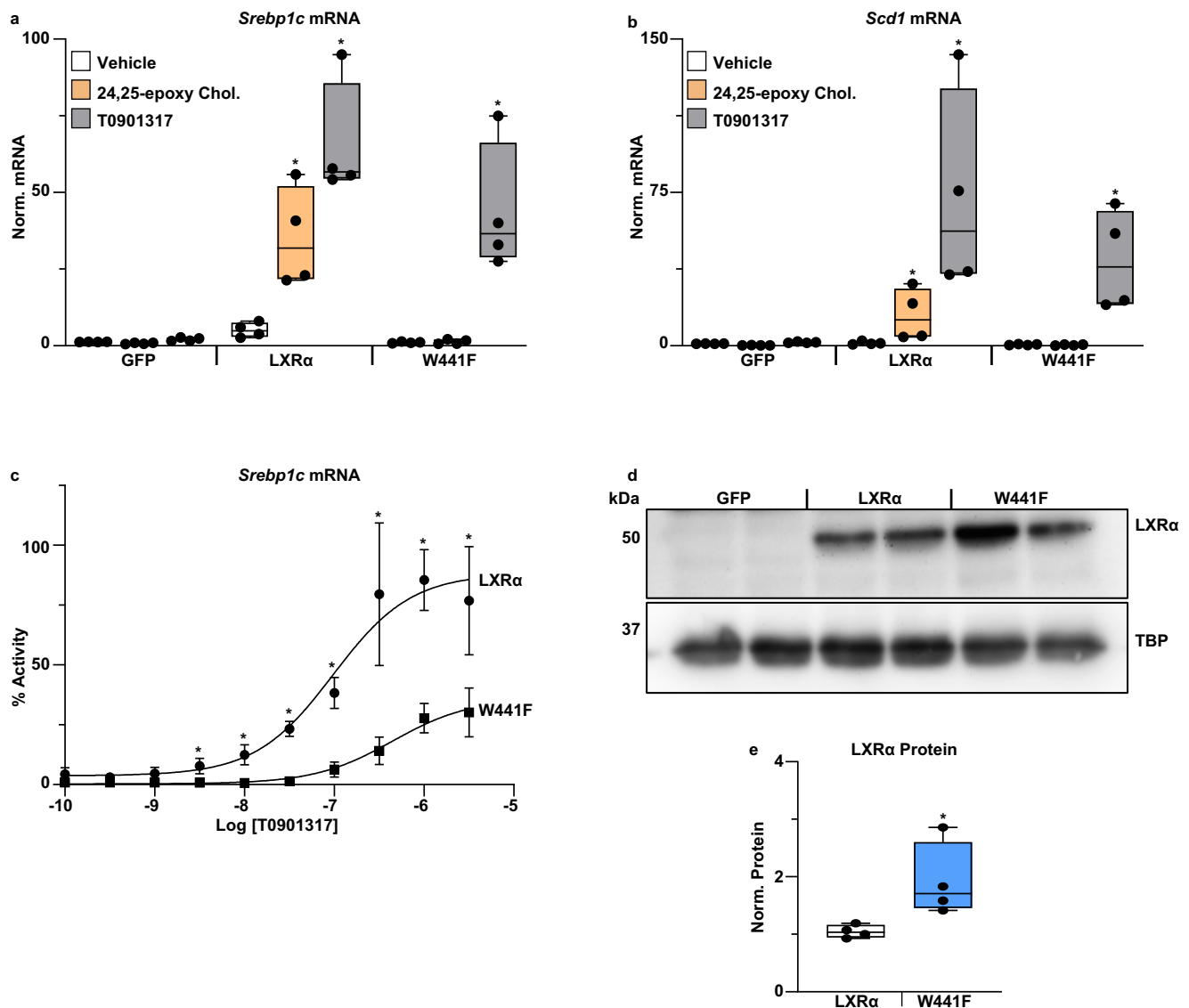


Fig. 1 | Characterization of LXRA W441F in vitro. Immortalized bone marrow derived macrophages were infected with adenovirus expressing LXRA or LXRA W441F. After infection, cells were treated for 24 h with 10 μ M 24(s),25-epoxycholesterol or 1.0 μ M T0901317. RNA was isolated and the mRNA levels of **a** *Srebp1c* and **b** *Scd1* were measured by real-time PCR as described in the Methods section. *Statistically significant difference between vehicle and treated group for each virus determined by two-way ANOVA ($p \leq 0.05$, $n = 4$). Each point represents an independent experiment with mRNAs measured in triplicate. Boxes extend from the 25th to 75th percentiles. The center line in the middle of the boxes represents the median. Whiskers extend from the lowest to the highest point. **c** Cells were infected as described above and treated with different concentrations of T0901317 for 24 h. RNA was isolated and *Srebp1c* mRNA levels were measured by real-time PCR as described in the Methods section. Data is the average of 3 independent

experiments with *Srebp1c* mRNA measured in duplicate. Error bars represent the standard deviation. *Statistically significant difference between LXRA and W441F determined by two-way ANOVA ($p \leq 0.05$, $n = 3$). **d** Nuclear extracts were prepared from immortalized bone marrow derived macrophages 24 h after infection. LXRA and TBP levels were examined by Western blotting. **e** LXRA protein levels were quantified from Western by normalization to TBP using ImageQuant TL. Each point is an individual infection. The amount of wildtype LXRA was set at 1. *Statistically significant difference between LXRA and W441F determined by two-tailed Mann-Whitney test ($p \leq 0.05$, $n = 4$). Boxes extend from the 25th to 75th percentiles. The center line in the middle of the boxes represents the median. Whiskers extend from the lowest to the highest point. Source data are provided as Source Data file.

transferase (AST) are elevated in plasma from F/F mice, indicative of liver damage (Supplemental Fig. 3b, c).

To further explore differences in hepatic gene expression among the 3 genotypes RNA-Sequencing (RNA-Seq) was used. Principle component analysis (PCA) of liver gene expression indicates that W/F heterozygotes more closely resemble W/W controls than heterozygous F/F mutants (Fig. 4a). Compared to W/W controls, 59 genes are mis-regulated in heterozygous W/F livers (39 down and 20 up). Gene ontology analysis indicates that most of the downregulated genes are linked to fatty acid metabolism (Fig. 4b) and 18 are either well-established LXR target genes or genes that have nearby LXR binding

sites identified by chromatin immunoprecipitation sequencing⁵⁶. The only significant upregulated pathways in W/F mice include 4 genes induced 2–2.3 fold that are associated with sterol metabolism. In contrast, over 2000 genes are differentially expressed in F/F homozygous mutant livers compared to W/W controls (488 down and 1688 up). Downregulated genes in F/F livers are also largely linked to fatty acid metabolism. Major gene networks selectively upregulated in F/F livers include those associated with cell division, inflammation/immune cell function, and cell adhesion/extracellular matrix (Fig. 4b). Representative changes in gene expression were confirmed by quantitative PCR (Fig. 4c–h). Increased expression of the chemokine

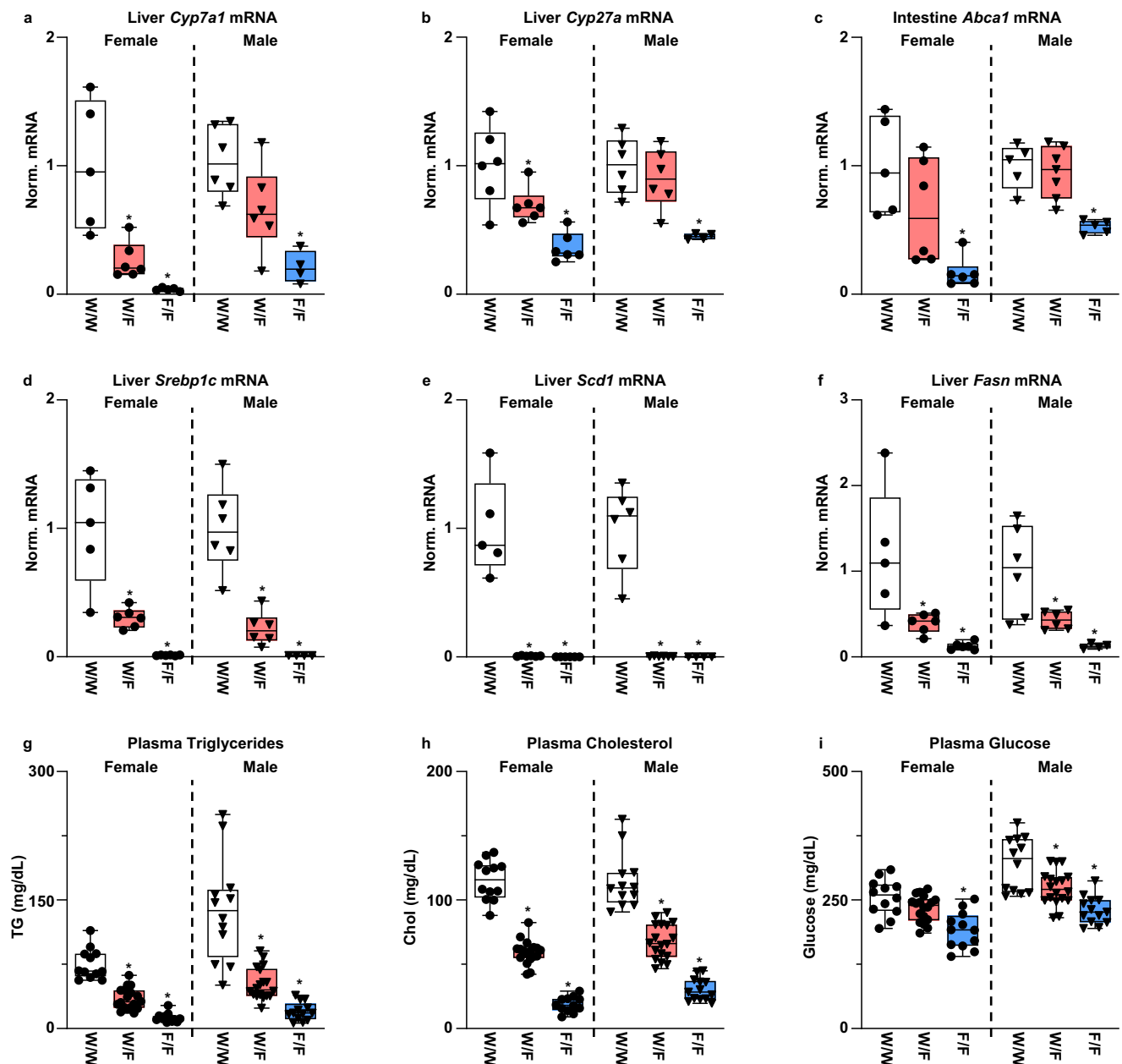


Fig. 2 | Gene expression and plasma lipids in LXRα W441F mice. Liver RNA, intestine RNA and plasma were isolated from 11–12 week old control (W/W), heterozygous mutant (W/F), and homozygous mutant (F/F) W441F mice maintained on normal chow diet. **a–f** Gene expression measured by real-time PCR as described in the Methods section. *Statistically significant difference between control and mutant mice determined by one-way ANOVA ($p \leq 0.05$; $n = 6$ W/W/sex, $n = 6$ W/F/sex, $n = 6$ F/F females, $n = 4$ F/F males). **g–i** Plasma triglycerides, cholesterol, and

glucose were measured as described in the Methods section. *Statistically significant difference between control and mutant mice determined by one-way ANOVA ($p \leq 0.05$; $n = 12$ W/W/sex, $n = 17$ W/F females, $n = 18$ W/F males, $n = 12$ F/F females, $n = 13$ F/F males). Boxes extend from the 25th–75th percentiles. The center line in the middle of the boxes represents the median. Whiskers extend from the lowest to the highest point. Source data are provided as Source Data file.

receptor *Cx3cr1* (Fig. 4c) along with elevated expression of pro-inflammatory genes such as *Tnf* (Fig. 4d) is consistent with the immune infiltration observed by H&E staining and suggests a pro-inflammatory environment in homozygous F/F mutant livers. Immunohistochemical staining with antibodies recognizing the macrophage marker Cd68 also detects increased numbers of macrophage in F/F mutant livers (Fig. 4i). Furthermore, several genes reported to be markers of lipid-associated macrophage populations defined in models of MASH and other chronic disease settings including *Trem2*, and *Spp1*^{57–59} are increased in F/F livers (Fig. 4e, f) while expression of Kupffer cell markers such as *Clec4e*^{60–63} are decreased (Fig. 4i). The decrease in Kupffer cell markers detected in homozygous F/F mutant mice is

supported by previous studies identifying LXRα as a lineage determining factor for this cell type^{60–62} and suggests sterol-dependent signaling is required for this function. Similar differences in gene expression are observed when RNA is isolated from an enriched population of liver macrophages (Supplemental Fig. 4a–d). The changes in macrophage gene expression suggest that LXR signaling is required for the proper specification and function of liver myeloid populations. By phagocytosing dead and dying cells throughout the body, macrophages are required to respond to large increases in intracellular cholesterol levels. We observe significant enlargement of spleens in homozygous F/F mice which are characterized by the appearance of lipid-loaded macrophages as determined by

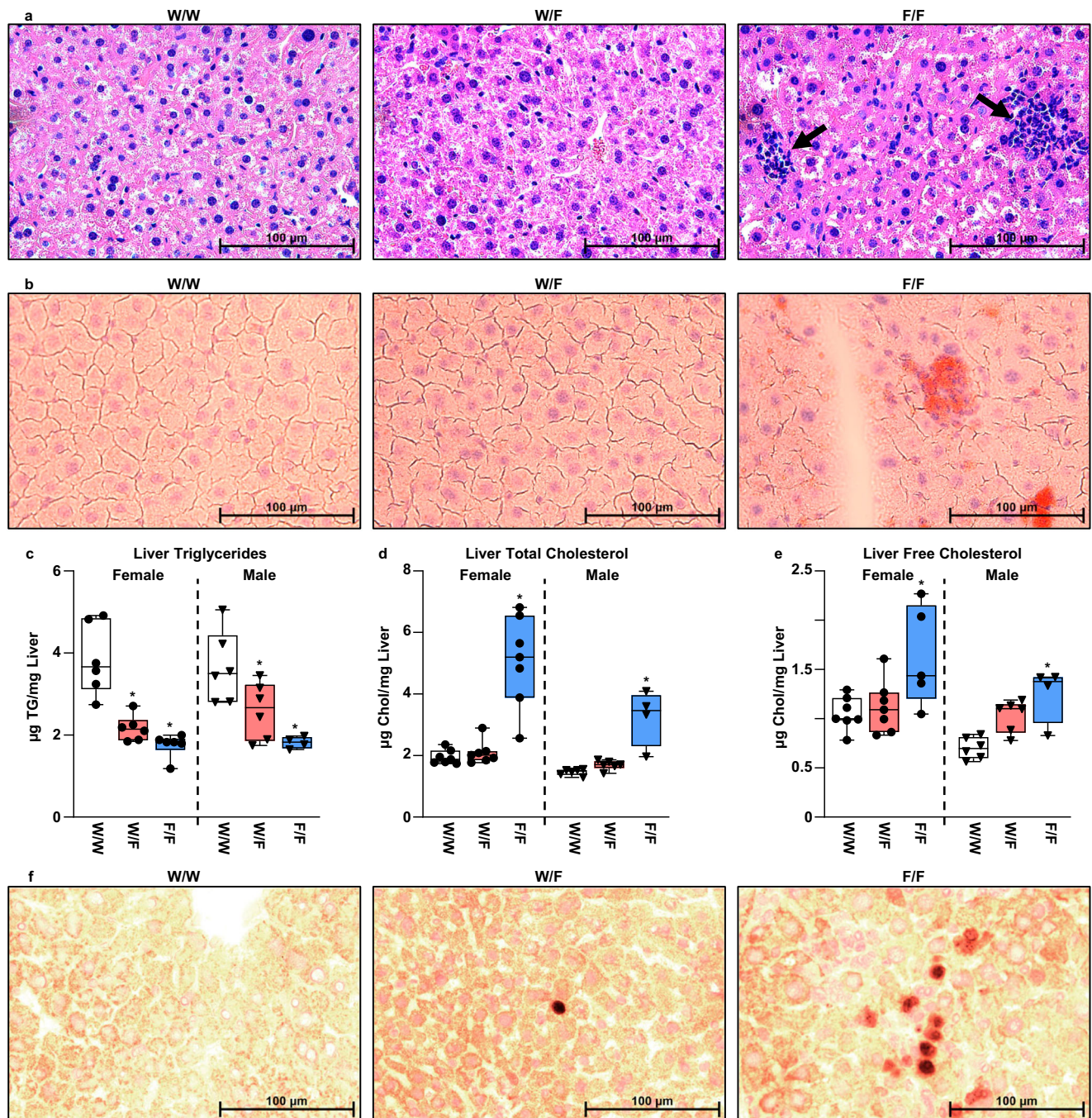


Fig. 3 | Cholesterol accumulation and increased cell division in *LXRα* W441F mice. **a** H&E and **b** Oil Red O staining of liver sections from representative male 11–12 week old control (W/W), heterozygous mutant (W/F), and homozygous mutant (F/F) W441F mice maintained on normal chow diet. Black arrows mark location of immune infiltration. **c–e** liver triglycerides and cholesterol were measured in samples from 11–12 week old control (W/W), heterozygous mutant (W/F), and homozygous mutant (F/F) W441F mice maintained on normal chow diet as described in Methods. *Statistically significant difference between control and

mutant mice determined by one-way ANOVA ($p \leq 0.05$; $n = 6$ W/W/sex, $n = 6$ W/F/sex, $n = 6$ F/F females, $n = 4$ F/F males). Boxes extend from the 25th–75th percentiles. The center line in the middle of the boxes represents the median. Whiskers extend from the lowest to the highest point. **f** Ki67 staining of representative liver sections from 11–12 week old male control (W/W), heterozygous mutant (W/F), and homozygous mutant (F/F) W441F mice maintained on normal chow diet. Source data are provided as Source Data file.

co-localization of Oil Red O staining with the macrophage marker Cd68 (Supplemental Fig. 4e–g). Thus, W441F mice uncover important roles for cholesterol sensing by LXRs in liver and splenic macrophage populations.

Rapid development of MASH phenotypes

On the normal mouse diet, heterozygous F/F mutant livers express many phenotypes associated with MASH including lipid loaded

hepatocytes, immune infiltration, and pro-fibrotic gene expression (e.g., *Spp1*, *Col1a1*, *Tgfb1*, Fig. 4f–h). Nevertheless, deposition of extracellular matrix and histological evidence of fibrosis is not detected. To examine the requirement for LXR signaling under MASH-promoting conditions, 11-week-old W441F mice were fed a MASH-promoting diet (21% fat, 1.25% cholesterol, 34% sucrose) for 2 weeks. Representatives of each genotype were sacrificed at this time point while the remaining animals continued on diet and were treated with

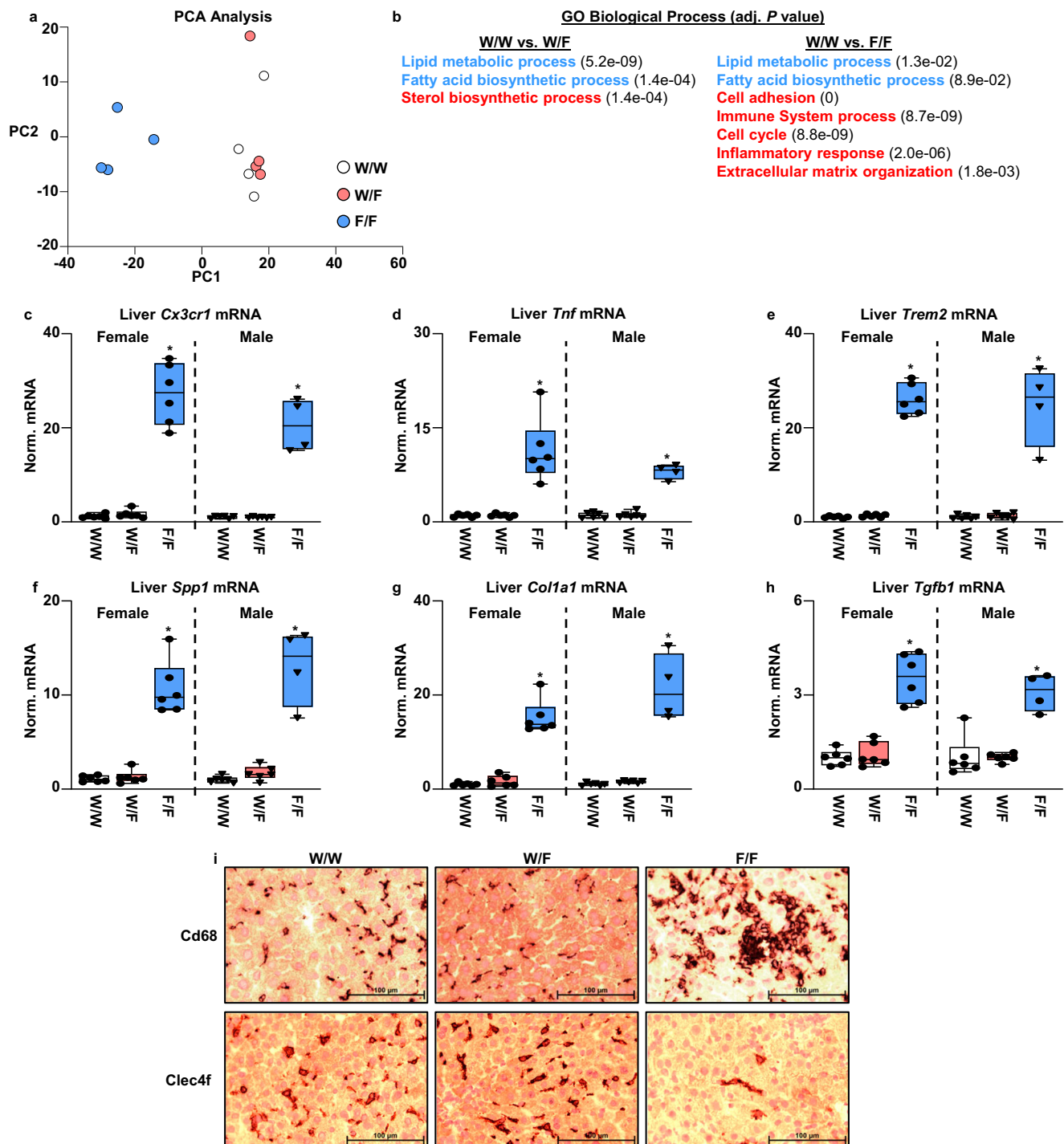
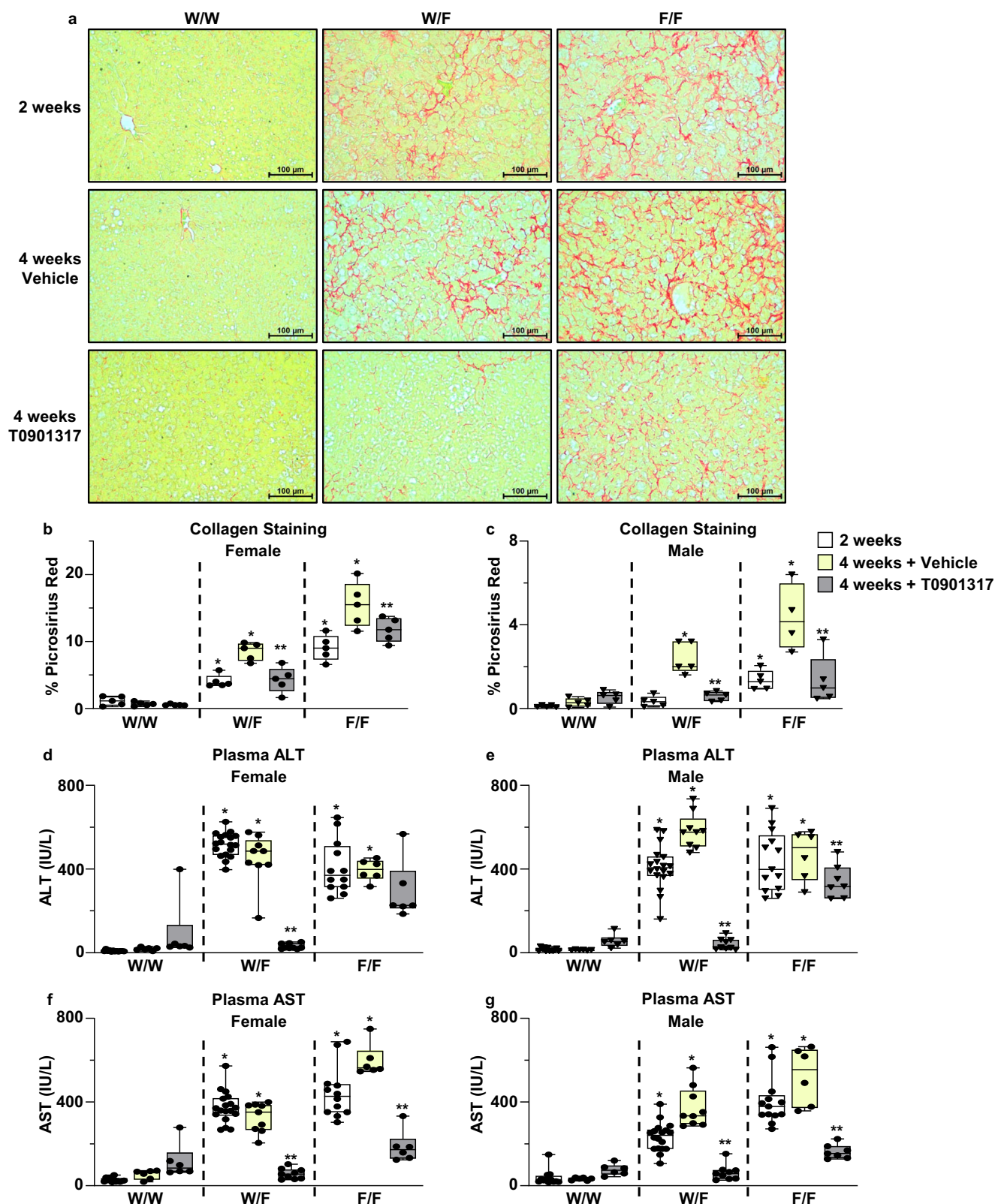


Fig. 4 | Liver gene expression in LXR α W441F mice. RNA-Seq was carried out as described in the Methods section using liver RNA isolated from 11–12 week old male control (W/W), heterozygous mutant (W/F), and homozygous mutant (F/F) W441F mice maintained on normal chow diet ($n = 4$ group). **a** PCA analysis. **b** Summary of enriched GO terms in pairwise comparisons. Blue = downregulated, red = upregulated. Adjusted *p* values were determined using Fisher exact test. **c–h** Gene expression measured by real-time PCR as described in the Methods section. *Statistically significant difference between control and mutant mice determined by

one-way ANOVA ($p \leq 0.05$; $n = 6$ W/W/sex, $n = 6$ W/F/sex, $n = 4$ F/F females, $n = 4$ F/F males). Boxes extend from the 25th–75th percentiles. The center line in the middle of the boxes represents the median. Whiskers extend from the lowest to the highest point. **i** Cd68 (top) and Clec4f (bottom) staining of representative liver sections from 11–12 week old female control (W/W), heterozygous mutant (W/F), and homozygous mutant (F/F) W441F mice maintained on normal chow diet. Source data are provided as Source Data file.

vehicle or with the LXR agonist T0901317 for an additional 2 weeks to reactivate LXR signaling (total of 4 weeks exposure to diet). After 2 weeks on diet, there is evidence of collagen deposition detected by Picrosirius Red staining in both heterozygous and homozygous W441F mice that further increases at 4 weeks in vehicle-treated mice

(Fig. 5a–c). Since most high fat/high cholesterol diet-dependent MASH models take several months to develop histologically detectable fibrosis^{15–17} the rapid development of fibrosis in W441F mice points to a critical role for LXR activity in regulating this process. Strikingly, collagen staining is reduced after reactivation of LXR signaling by



T0901317 compared to vehicle-treated animals and resembles the levels measured in animals at 2 weeks. Liver damage quantified by plasma ALT and AST activity follows a similar trajectory and is also strongly reduced by re-engaging LXR activity (Fig. 5d–g). Notably, liver enzymes are normalized in heterozygous W/F mutant mice.

Oil Red O staining of neutral lipids in liver sections from mice on the MASH diet (Fig. 6a) illustrates unique patterns of lipid

accumulation in W441F mice compared to controls. As typically observed in livers from mice fed high-fat diets, control W/W mice have relatively small intensely stained lipid droplets that increase in size between 2 and 4 weeks. Furthermore, treatment of control mice with the LXR agonist T0901317, known to promote fatty acid synthesis^{25,26}, increases the size of the droplets. In contrast, hepatocytes from heterozygous and homozygous W441F mice exhibit diffuse lipid staining

Fig. 5 | Fibrosis and liver damage in LXR α W441F mice. Female and male 11–12 week old control (W/W), heterozygous mutant (W/F), and homozygous mutant (F/F) W441F mice were fed the MASH diet. A subset of mice was sacrificed after 2 weeks. The remaining mice were maintained on the MASH diet for an additional 2 weeks and treated with vehicle or 10 mg/kg T0901317 daily by oral gavage as described in the Methods section. **a** Liver sections from representative female mice stained with Picrosirius Red to visualize collagen. **b, c** Quantification of the % surface area positive for Picrosirius Red in liver sections from female and male mice as described in the Methods section. *Statistically significant difference between control and mutant mice in the same treatment group; **statistically significant difference between vehicle and T0901317 treated mice of the same

genotype determined by two-way ANOVA ($p \leq 0.05$, $n = 5/\text{group}$). **d–g** Plasma ALT and AST levels. *Statistically significant difference between control and mutant mice in the same treatment group; **statistically significant difference between vehicle and T0901317 treated mice of the same genotype determined by two-way ANOVA ($p \leq 0.05$). 2 weeks: $n = 12$ W/W/sex, $n = 18$ W/F/sex, $n = 12$ F/F females and 13 F/F males. 4 weeks + vehicle: $n = 6$ W/W/sex, $n = 9$ W/F/sex, $n = 6$ F/F/sex. 4 weeks + T0901317: $n = 6$ W/W/sex, $n = 9$ W/F/sex, $n = 6$ F/F females and 7 F/F males. Boxes extend from the 25th–75th percentiles. The center line in the middle of the boxes represents the median. Whiskers extend from the lowest to the highest point. Source data are provided as Source Data file.

(Fig. 6a). The lipid-loaded cells in W441F mice appear to correlate with large ballooning hepatocytes detected in H&E stained liver sections (Fig. 6b) and we suggest that these cells are filled largely with cholesterol. Consistent with this hypothesis, liver cholesterol is elevated in W441F mice after 2 and 4 weeks of diet while liver triglycerides are decreased compared to W/W controls (Fig. 6c–f). Reactivation of LXR signaling by treatment with T0901317 reduces liver cholesterol in heterozygous W/F mutants but does not drive a significant reduction in homozygous F/F mice (Fig. 6). Livers from W441F mice are fibrotic (Supplemental Fig. 5a) and difficult to extract such that the amount of cholesterol and the effect of reactivating LXR may be underestimated particularly in F/F samples. Liver and spleen weights are also significantly increased in W441F mice after 2 and 4 weeks on the MASH diet and re-engaging LXR signaling by treatment with T0901317 either completely (W/F heterozygotes) or partially (F/F homozygous) rescues these phenotypes (Supplemental Fig. 5b–e). The increase in liver weight observed in W/W control mice treated with T0901317 is consistent with previous reports of this compound promoting hepatomegaly in high-fat-fed mice²⁶. Finally, W441F mutant mice fail to gain weight on the MASH diet and their fat mass is reduced (Supplemental Fig. 6). This failure to thrive appears to be secondary to liver damage and is reversed in T0901317 treated animals.

After 2 weeks on the MASH diet W/F heterozygote livers now phenotypically resemble F/F homozygous livers demonstrating increased hepatic cholesterol, immune infiltration, and collagen deposition. Changes in gene expression are an additional manifestation of the influence of diet on the heterozygous W/F phenotype. After 4 weeks on the MASH diet, PCA of liver RNA-Seq data indicates that liver gene expression in vehicle-treated W/F heterozygous mice now closely resembles the expression pattern observed in F/F homozygotes with 4030 and 5095 mis-regulated genes in W/F and F/F livers respectively (Fig. 7a). GO analysis identifies many of the same pathways seen mis-regulated in normal chow F/F mice including lipid metabolism, inflammation, and cell adhesion/extracellular matrix, however the magnitude of the changes in gene expression are greater after exposure to the MASH diet (Fig. 7b–j). Heterozygous W/F mutant mice are particularly responsive to T0901317 treatment and PCA of liver RNA-Seq data sets indicate that the transcriptome of LXR agonist-treated W/F heterozygotes closely mimics the transcriptome of vehicle-treated control W/W mice (Fig. 7a). The diet-dependent changes in liver gene expression measured in W/F heterozygotes uncovers a context selective haploinsufficiency of the W441F mutation. Strikingly, in mutant mice treated with T0901317 to reactivate LXR the MASH phenotypes including lipid accumulation, immune infiltration and fibrosis measured at the level of gene expression or by histology are largely reversed (Figs. 5–7).

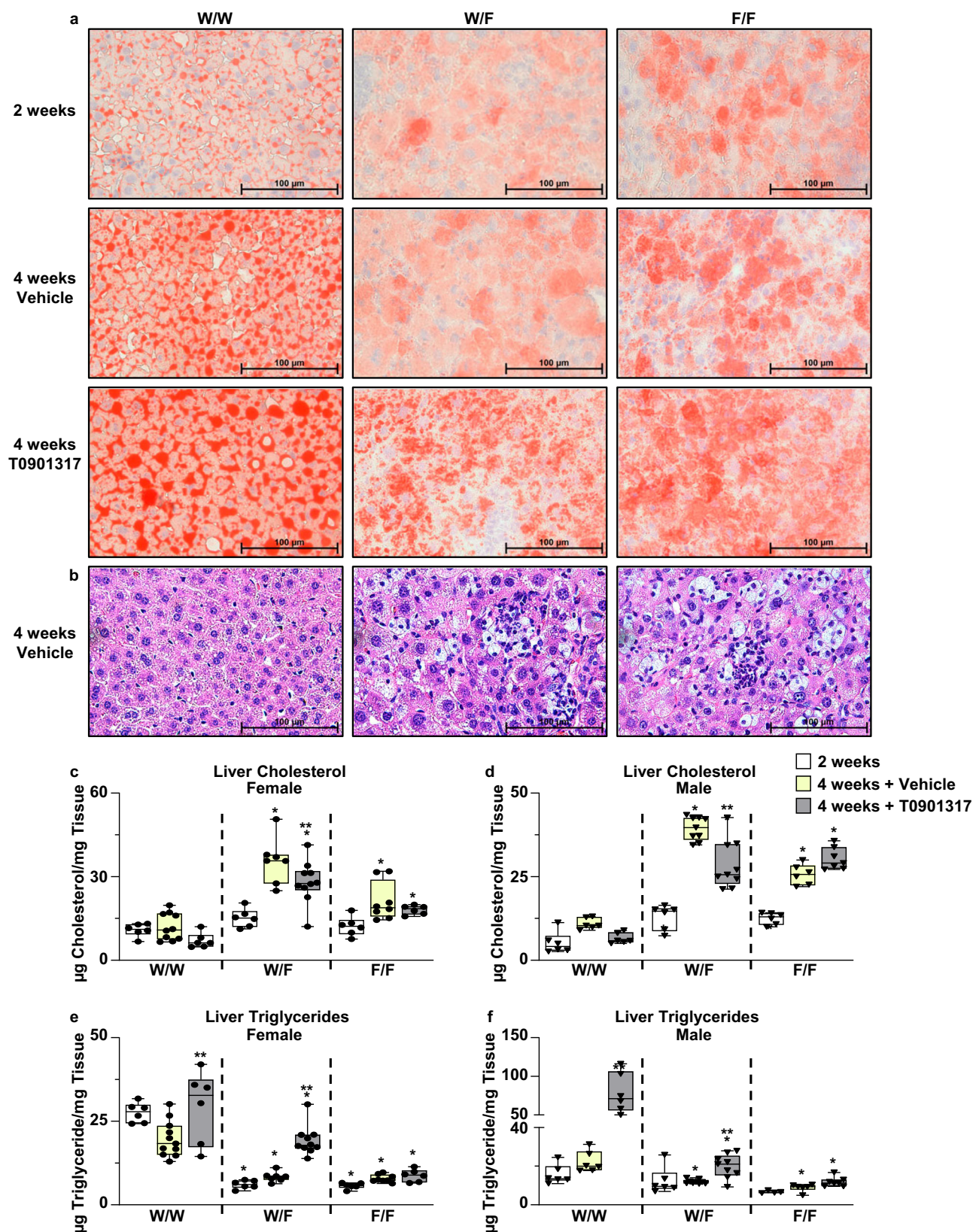
TAZ is a transcriptional coactivator that is over-expressed in human MASH patients and in mouse models^{64–66}. Recent studies indicate that TAZ is stabilized by elevated hepatic cholesterol and promotes fibrosis and inflammation^{66–68}. We do not detect differences in TAZ protein levels in livers from female control, heterozygous or homozygous W441F mice fed the MASH Diet (Supplemental Fig. 7a, b). In contrast, there is an increase in TAZ levels in livers from male W441F

mice (Supplemental Fig. 7c, d). Interestingly, the published studies exploring the contribution of TAZ to the development of MASH in mice have only examined male animals^{66–68}. Treatment of male mice with T0901317 for 2 weeks increases the amount of TAZ in control W/W mice (Supplemental Fig. 7c, d). Nevertheless, there is no histological evidence of inflammation or fibrosis in these animals. Therefore, in the W441F model increasing TAZ is not sufficient to promote MASH at least after 4 weeks of exposure to a MASH diet.

Using an independent cohort of male mice we directly compared the phenotypes observed in LXR α W441F mutants to LXR α knockout (*Lxra*^{−/−})²² mice after 4 weeks on the MASH diet. LXR target genes are downregulated in *Lxra*^{−/−} mice relative to homozygous W/W control mice, however the decreases in mRNA levels are not as pronounced as measured in LXR α W441F mutants (Fig. 8a–d). Consistent with decreased LXR-dependent gene expression, liver cholesterol is increased and liver triglycerides are decreased in *Lxra*^{−/−} mice (Fig. 8e–g). Increased macrophage content measured by *Cd68* mRNA (Fig. 8f) and immunohistochemistry (Supplemental Fig. 8a) is apparent in *Lxra*^{−/−} mice and can also be detected in H&E stained liver sections (Supplemental 8b). Nevertheless, molecular markers of MASH including mRNA levels of *Trem2* and *Col1a1* as well as liver enzymes (Fig. 8i–k) are higher in W441F mutants when compared to *Lxra*^{−/−} mice. Other phenotypes including decreased expression of Kupffer cell markers, increased cell division, elevated liver and spleen to body weight ratios, and decreased body weight gain follow a similar trend of being less severe in *Lxra*^{−/−} mice (Supplemental Fig. 8c–h). Consistent with the less severe MASH phenotypes, collagen staining is not increased in *Lxra*^{−/−} mice after 4 weeks on the MASH diet (Fig. 8l, m). Overall, the effect of deleting LXR α is quantitatively less severe than expression of the dominant negative W441F mutant and the knockout does not lead to the same accelerated development of fibrosis. Genetic deletion of LXR α , however, does generate a pro-inflammatory and profibrotic environment that may favor the development of fibrosis over a slightly longer time frame.

Hepatocyte-specific expression of W441F drives MASH

LXR α is expressed in all the cell-types that contribute to MASH including hepatocytes, Kupffer cells, infiltrating macrophages, and hepatic stellate cells¹⁹. Aberrant lipid accumulation in hepatocytes, however, is thought to be the original insult driving MASH in humans and in mouse models^{2,3,69}. To determine if expression of LXR α W441F selectively in hepatocytes is sufficient to promote MASH phenotypes in mice we used CRISPR to integrate a trans-gene expressing FLAG tagged LXR α W441F under control of a Cre-dependent Lox-Stop-Lox cassette at the *Rosa26* locus. The *Rosa26* insertion was crossed into *Lxra*^{fl/m} mice²³ such that Cre promotes expression of LXR α W441F while simultaneously excising the wildtype allele. To selectively express W441F in hepatocytes *Rosa26* W441F + *Lxra*^{fl/m} mice were infected with adeno associated virus (AAV) expressing GFP or Cre under control of the hepatocyte-specific thyroxine binding globulin (TBG) promoter (Fig. 9a). Following infection, mice were maintained on a normal chow diet for 2 weeks before being switched to the MASH diet for an additional 4 weeks. Western blotting of liver nuclear extracts indicates that



mice infected with TBG-Cre express ~10 times more FLAG-W441F protein than TBG-GFP controls (Fig. 9b and Supplemental Fig. 9a). After 4 weeks on the MASH diet, mice expressing W441F in hepatocytes demonstrate essentially the same phenotypes observed in mice expressing W441F from the endogenous locus including lipid loaded ballooning hepatocytes (Fig. 9c, d), decreased liver triglycerides

(Fig. 9e), increased liver cholesterol (Fig. 9f), diffuse lipid staining (Fig. 9g, h), increased collagen deposition (Fig. 9i–k), elevated liver enzymes (Fig. 9l), and enlarged livers (Supplemental Fig. 9b). Hepatocyte-selective W441F mice also fail to gain weight (Supplemental Fig. 9c, d) indicating that this phenotype is autonomous to hepatocytes and is most likely a secondary effect of liver damage.

Fig. 6 | Lipid accumulation in livers from LXR α W441F mice fed the MASH diet. Female and male 11–12 week old control (W/W), heterozygous mutant (W/F), and homozygous mutant (F/F) W441F mice were fed the MASH diet. A subset of mice was sacrificed after 2 weeks. The remaining mice were maintained on the MASH diet for an additional 2 weeks and treated with vehicle or 10 mg/kg T0901317 daily by oral gavage as described in the Methods section. Representative liver sections from female mice stained with **a** Oil Red O and **b** H&E. **c–f** Liver cholesterol and triglyceride levels measured as described in the Methods section. *Statistically significant difference between control and mutant mice in the same treatment group;

**statistically significant difference between vehicle and T0901317 treated mice of the same genotype determined by two-way ANOVA ($p \leq 0.05$). 2 weeks: $n = 6/\text{group}$. 4 weeks + vehicle: W/W = 10 females and 6 males, W/F = 7 females 9 males, F/F = 8 females and 6 males. 4 weeks + T0901317: W/W = 6/sex, W/F = 7 females and 9 males, F/F = 6 females and 7 males. Boxes extend from the 25th–75th percentiles. The center line in the middle of the boxes represents the median. Whiskers extend from the lowest to the highest point. Source data are provided as Source Data file.

Direct LXR target genes such as *Srebp1c* and *Abcg5* are downregulated (Fig. 9m, n). Conversely, markers of infiltrating macrophages, lipid-associated macrophages, fibrosis, and cell division are upregulated (Fig. 9o–t). Cre-dependent changes in gene expression are not observed in the intestine (Supplemental Fig. 9e–g). The characterization of hepatocyte-selective W441F mice indicates that inhibiting LXR transcriptional activity in hepatocytes is sufficient to rapidly promote phenotypes associated with MASH.

Kupfer cells are liver resident macrophages derived from the embryonic yolk sac and previous studies have identified LXR α as a lineage specifying transcription factor for this cell type^{61,62}. Genetic deletion of LXR α in Kupffer cells leads to a loss of embryonic-derived cells and replacement with monocyte-derived “Kupffer-like” cells that are positive for the Kupffer cell marker *Clec4f* and negative for the marker *Tim4d*^{61,62}. A similar replacement of embryonic-derived Kupffer cells with *Clec4f*⁺/*Tim4d*[−] monocyte-derived cells is seen in mouse models of MASH and in human MASH patients^{58,59,61,62}. To examine the consequence of selectively expressing LXR α W441F in Kupffer cells we generated *Rosa26* Lox-Stop-Lox W441F + *Lxr α ^{W441F}* + *Clec4f*-Cre-tdTomato mice (Fig. 10a, b) and placed male *Cre^{+/+}* and *Cre^{−/−}* littermates on the MASH diet for 4 weeks. Consistent with a role for LXR α in Kupffer cell determination, we detect decreased expression of *Clec4f* and *Tim4d* in *Cre^{+/+}* mice by histochemical staining of liver sections and in total liver RNA (Fig. 10c–f). In contrast, LXR target genes that are expressed in multiple cell types (*Srebp1c*) or that are restricted to hepatocytes (*Abcg5*) show no difference when *Cre^{+/+}* and *Cre^{−/−}* mice are compared (Fig. 10g, h). Despite the decrease in Kupffer cells, there is no evidence for lipid accumulation, liver damage, macrophage infiltration, inflammation, or profibrotic gene expression when *Cre^{+/+}* and *Cre^{−/−}* animals are compared (Fig. 10i–o). Liver triglycerides are slightly reduced in *Cre^{+/+}* mice compared to *Cre^{−/−}* controls (Fig. 10j) which is consistent with published studies demonstrating that replacement of embryonic-derived Kupffer cells with monocyte-derived cells lowers liver triglycerides⁶³. Finally, Kupffer cell-selective expression of LXR α W441F does not lead to changes in body weight or liver weight (Supplemental Fig. 10) as observed in hepatocyte-selective W441F mice. Taken together, the characterization of cell-type selective W441F mice highlights a critical role for LXR activity in hepatocytes controlling inflammation and fibrosis in response to a MASH-promoting diet.

Discussion

MASH is rapidly becoming the leading cause of liver disease, liver failure, and hepatocellular carcinoma in humans¹. Although steatotic liver disease (fatty liver) is reaching epidemic proportions due to the rise in obesity¹, what drives the transition of steatosis to the inflammation and fibrosis characteristic of MASH is not known. LXR α is an intracellular cholesterol sensor that regulates lipid metabolism at the transcriptional level in response to the direct binding of cholesterol derivatives¹⁹. We demonstrate that disrupting the ability of LXR α to sense cholesterol generates a dominant negative transcription factor (W441F) that inhibits LXR-dependent transcription even when present in a heterozygous state. Within 2 weeks of exposure to a high-fat, high-cholesterol MASH-promoting diet W441F mice develop the hallmarks of human MASH including lipid-laden ballooning hepatocytes,

elevated liver enzymes, inflammation, and fibrosis. W441F impairs the transcriptional response to endogenous cholesterol-derived ligands, however, the mutant receptor can still activate transcription in response to potent synthetic agonists such as T0901317. Importantly, reactivation of LXR signaling after 2 weeks of the MASH diet blocks the further progression of fibrosis and either completely (heterozygotes) or partially (homozygotes) reverses liver damage and inflammation. W441F mice accumulate high levels of hepatic cholesterol highlighting the potential pathological role of cholesterol in MASH. The cholesterol-associated steatohepatitis (CASH) observed in W441F mice is consistent with studies in humans linking the severity of MASH with hepatic cholesterol levels^{5,6,8}. Hepatic triglycerides on the other hand are generally lower in W441F mice compared to controls. Nevertheless, hepatic triglycerides are increased when W441F mice on the MASH diet are compared to mice of the same genotype on the normal chow diet. Therefore, elevated high hepatic triglycerides may also be necessary for MASH to develop in W441F mice. Since LXR α regulates cholesterol excretion and catabolism in hepatocytes¹⁹, it is likely that restoration of these activities contributes to the beneficial effects reactivating W441F with synthetic agonists. In heterozygous W/F mice on the MASH diet treatment with LXR agonist reduces hepatic cholesterol by approximately 25%. In homozygous F/F mutants, however, there is no apparent effect of agonist treatment on hepatic cholesterol. While this negative result may reflect difficulty in extracting cholesterol from fibrotic livers, we cannot rule out the possibility that other LXR activities contribute to reversing MASH. For instance, LXR agonists also elicit anti-inflammatory activity which could play a role in reversing MASH^{41,44,70,71}. Future studies that individually dissect these pathways will be useful for identifying therapeutic targets for treating MASH.

LXR α is also a well-established transcriptional regulator of fatty acid synthesis and inhibition of LXR activity with synthetic antagonists has been suggested as a therapeutic approach for treating steatotic liver disease²⁷. Our finding that inhibiting endogenous LXR activity accelerates the development of MASH seems at odds with the use of LXR antagonists as MASH therapeutics. Consistent with our studies, Lockhart et al.⁴⁰ recently identified rare inactivating point mutations in the human LXR α gene including a patient with mutation of tryptophan 443 to arginine (W443 is equivalent to mouse W441). Patients with LXR inactivating mutations demonstrate an increased risk for liver damage and the W441R mouse develops MASH. There are several possible explanations that may help align genetic data suggesting LXR activity protects the liver with the beneficial effects seen with LXR antagonists in models of steatosis and MASH. First, it is difficult to compare the constitutive dominant negative effect of W441F to the activity of small molecules with defined half-lives and clearance mechanisms. Completely shutting off LXR activity genetically may prove detrimental while partial or incomplete pharmacological inhibition may be beneficial. Second, we have observed that LXR target genes regulating fatty acid synthesis are more sensitive to LXR α inactivation than target genes regulating cholesterol metabolism (Fig. 2). Therefore, synthetic antagonists may preferentially inhibit fatty acid synthesis which could be beneficial in MASH without promoting cholesterol accumulation which our study suggests could be detrimental. A less likely explanation that aligns the discordant genetic

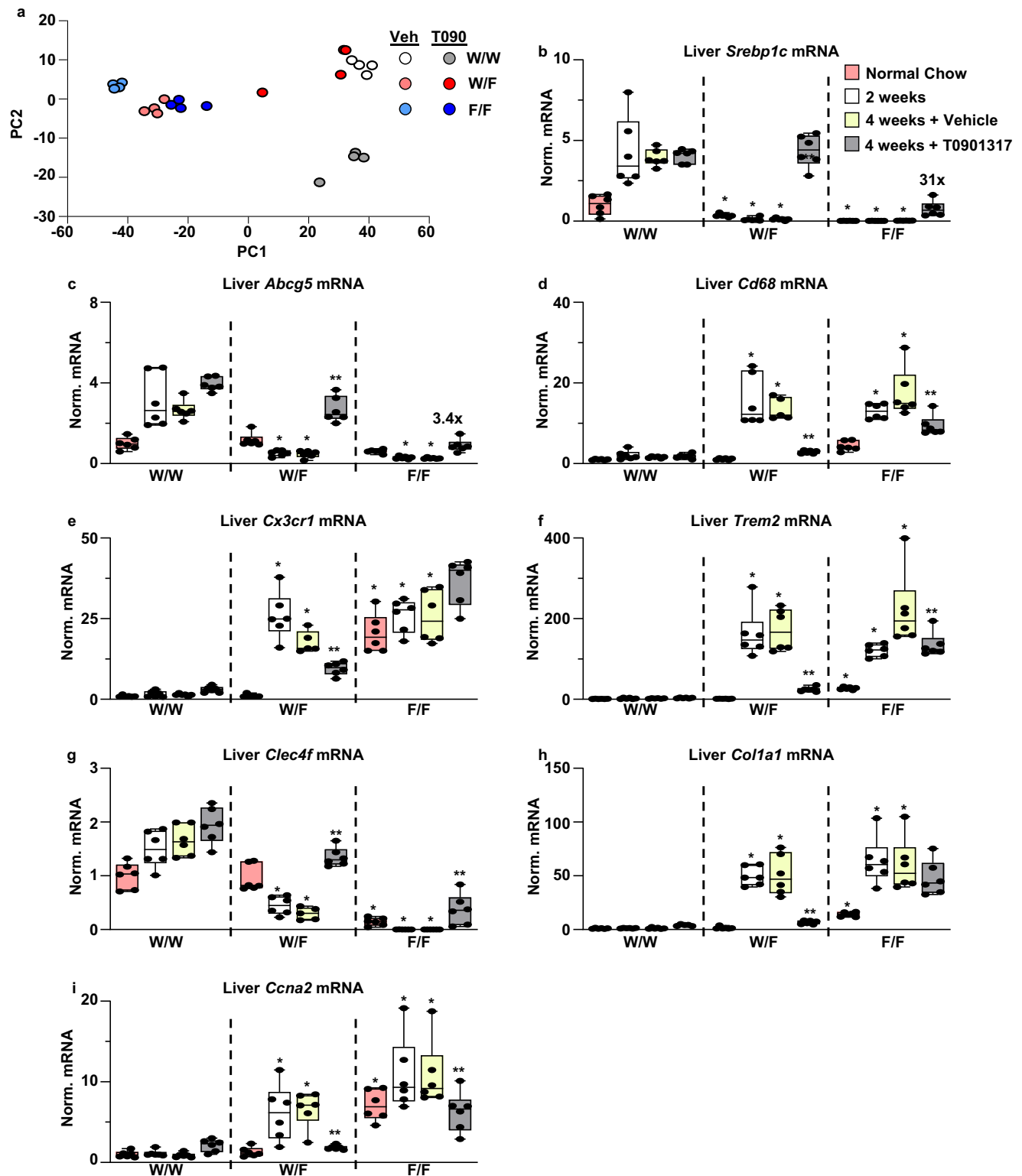


Fig. 7 | Liver gene expression in LXR α W441F mice fed the MASH diet. Female and male 11–12 week old control (W/W), heterozygous mutant (W/F), and homozygous mutant (F/F) W441F mice were fed the MASH diet. A subset of mice was sacrificed after 2 weeks. The remaining mice were maintained on the MASH diet for an additional 2 weeks and treated with vehicle or 10 mg/kg T0901317 daily by oral gavage as described in the Methods section. **a** PCA analysis of RNA-Seq data using liver RNA isolated from male mice ($n = 4$ /group). **b–i** Gene expression in livers from female mice measured by real-time PCR as described in the Methods section. Gene expression was also measured in an independent cohort of 11–12 week old female

mice maintained on normal chow. Numbers in **b** and **c** represent the fold induction by T0901317 in F/F mice. *Statistically significant difference between control and mutant mice in the same treatment group; **statistically significant difference between vehicle and T0901317 treated mice of the same genotype determined by two-way ANOVA ($p \leq 0.05$, $n = 6$ /group). Boxes extend from the 25th–75th percentiles. The center line in the middle of the boxes represents the median. Whiskers extend from the lowest to the highest point. Source data are provided as Source Data file.

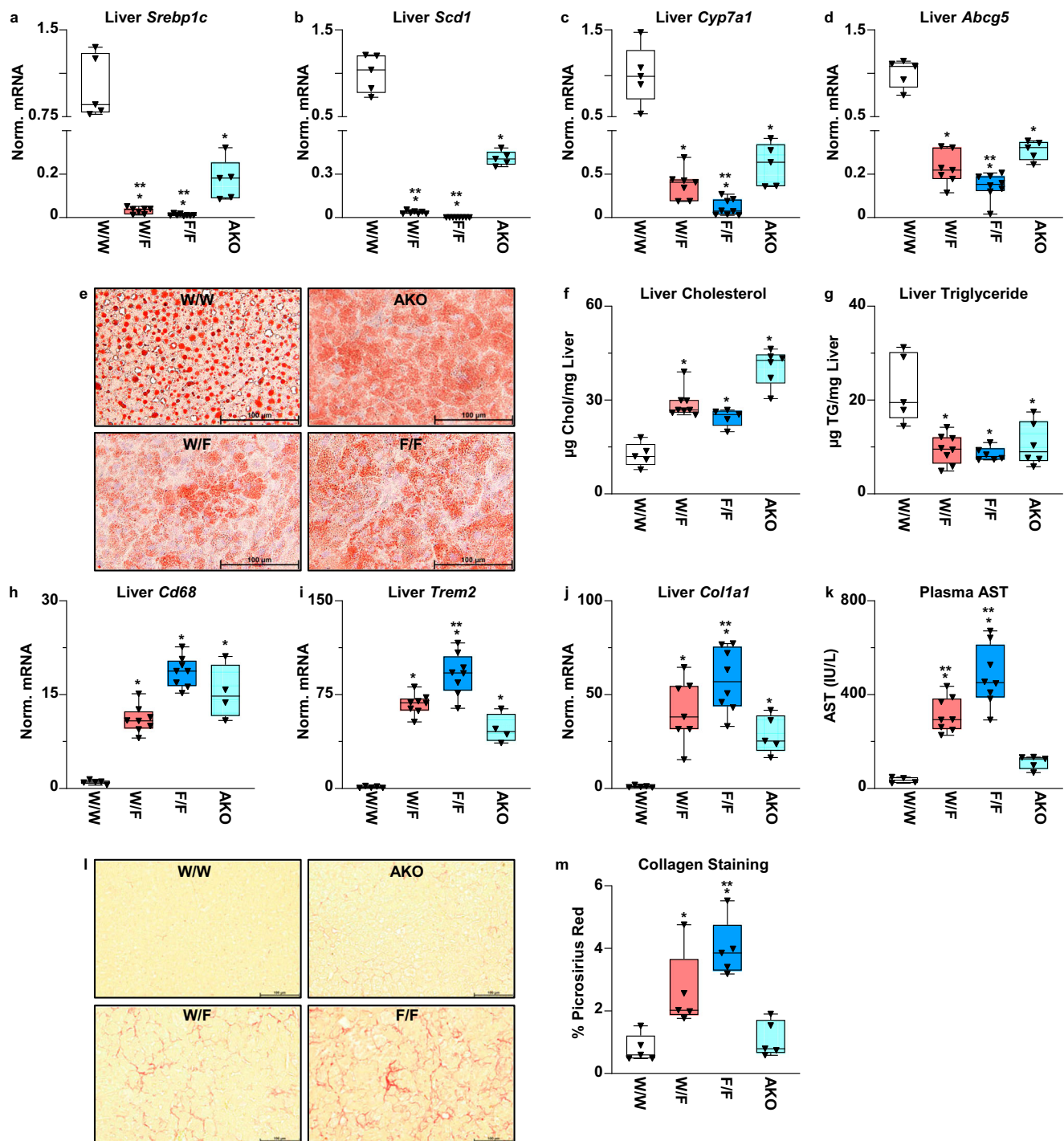


Fig. 8 | Comparison of LXRα W441F and LXRα knockout mice. Male 11–13 week old control (W/W), heterozygous (W/F), homozygous (F/F) W441F mice and *Lxrα*^{-/-} mice (AKO) were fed the MASH diet for 4 weeks. **a–d** Liver gene expression measured by real-time PCR. *Statistically significant difference between control (W/W) and mutant mice; **statistically significant difference between AKO and W441F mutant mice determined by one-way ANOVA ($p \leq 0.05$, W/W = 5, W/F = 7, F/F = 8, AKO = 5). **e** Representative Oil Red O stained liver sections. **f, g** Liver cholesterol and triglycerides. *Statistically significant difference between control (W/W) and mutant mice; **statistically significant difference between AKO and W441F mutant mice determined by one-way ANOVA ($p \leq 0.05$, W/W = 5, W/F = 8, F/F = 5, AKO = 6). **h–j** Liver gene expression measured by real-time PCR. *Statistically significant difference between control (W/W) and mutant mice; **statistically significant

difference between AKO and W441F mutant mice determined by one-way ANOVA ($p \leq 0.05$, W/W = 5, W/F = 7, F/F = 8, AKO = 4). **k** Plasma AST. *Statistically significant difference between control (W/W) and mutant mice; **statistically significant difference between AKO and W441F mutant mice determined by one-way ANOVA ($p \leq 0.05$, W/W = 5, W/F = 7, F/F = 8, AKO = 5). **l** Representative Picrosirius Red stained liver sections. **m** Quantification of the % surface area positive for Picrosirius Red. *Statistically significant difference between control (W/W) and mutant mice; **statistically significant difference between AKO and W441F mutant mice determined by one-way ANOVA ($p \leq 0.05$, $n = 5$ /group). For all whisker plots in the figure, boxes extend from the 25th–75th percentiles. The center line in the middle of the boxes represents the median. Whiskers extend from the lowest to the highest point. Source data are provided as Source Data file.

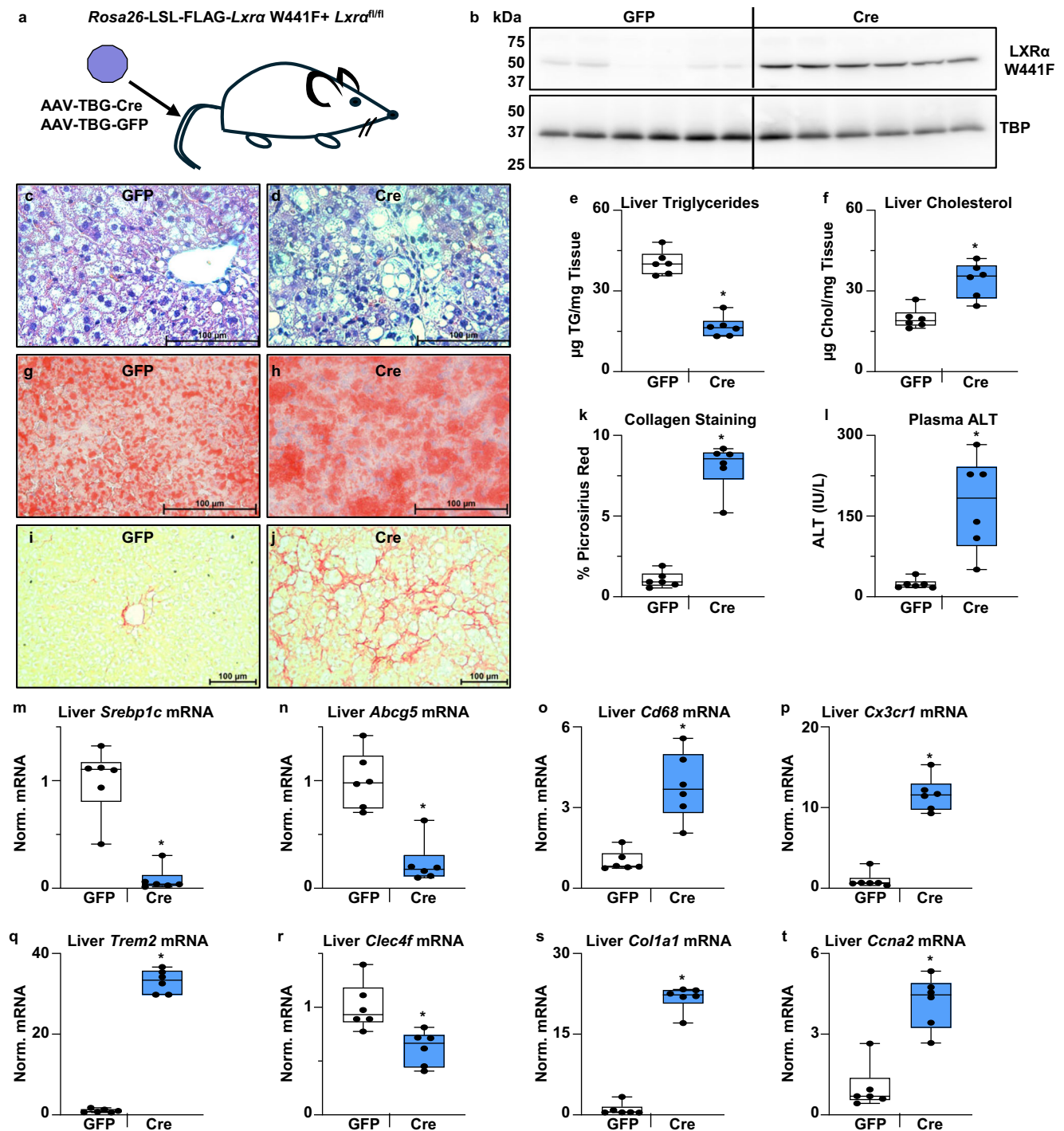


Fig. 9 | Hepatocyte-selective expression of LXRA W441F promotes MASH.

Female 9 week old *Rosa26-LSL-FLAG-LXRA* W441F/*Lxra*^{fl/fl} mice were infected with AAV-TBG-GFP or AAV-TBG-Cre viruses. Mice were maintained on a normal chow diet for 2 weeks and then fed the MASH diet for 4 weeks. **a** Experimental schematic. **b** Liver nuclear extracts were prepared as described in the Methods. FLAG-LXRA and TBP levels were examined by Western blotting. **c, d** Representative H&E stained liver sections. **e, f** Liver triglycerides and cholesterol were measured as described in the methods section. *Statistically significant difference between GFP and Cre mice determined by unpaired two-tailed *t*-test ($p \leq 0.05$, $n = 6/\text{group}$). **g, h** Representative Oil Red O stained liver sections. **i, j** Representative Picrosirius Red stained liver sections. **k** Quantification of the % surface area positive for

Picrosirius Red in liver sections as described in the Method section. *Statistically significant difference between GFP and Cre mice determined by unpaired two-tailed *t*-test ($p \leq 0.05$, $n = 6/\text{group}$). **l** Plasma ALT measured as described in the Methods section. *Statistically significant difference between GFP and Cre mice determined by two-tailed Mann-Whitney tests ($p \leq 0.05$, $n = 6/\text{group}$). **m–t** Liver gene expression measured by real-time PCR as described in the Methods section. *Statistically significant difference between GFP and Cre mice determined by unpaired two-tailed *t*-test or two-tailed Mann-Whitney test ($p \leq 0.05$, $n = 6/\text{group}$). For all whisker plots in the figure, boxes extend from the 25th–75th percentiles. The center line in the middle of the boxes represents the median. Whiskers extend from the lowest to the highest point. Source data are provided as Source Data file.

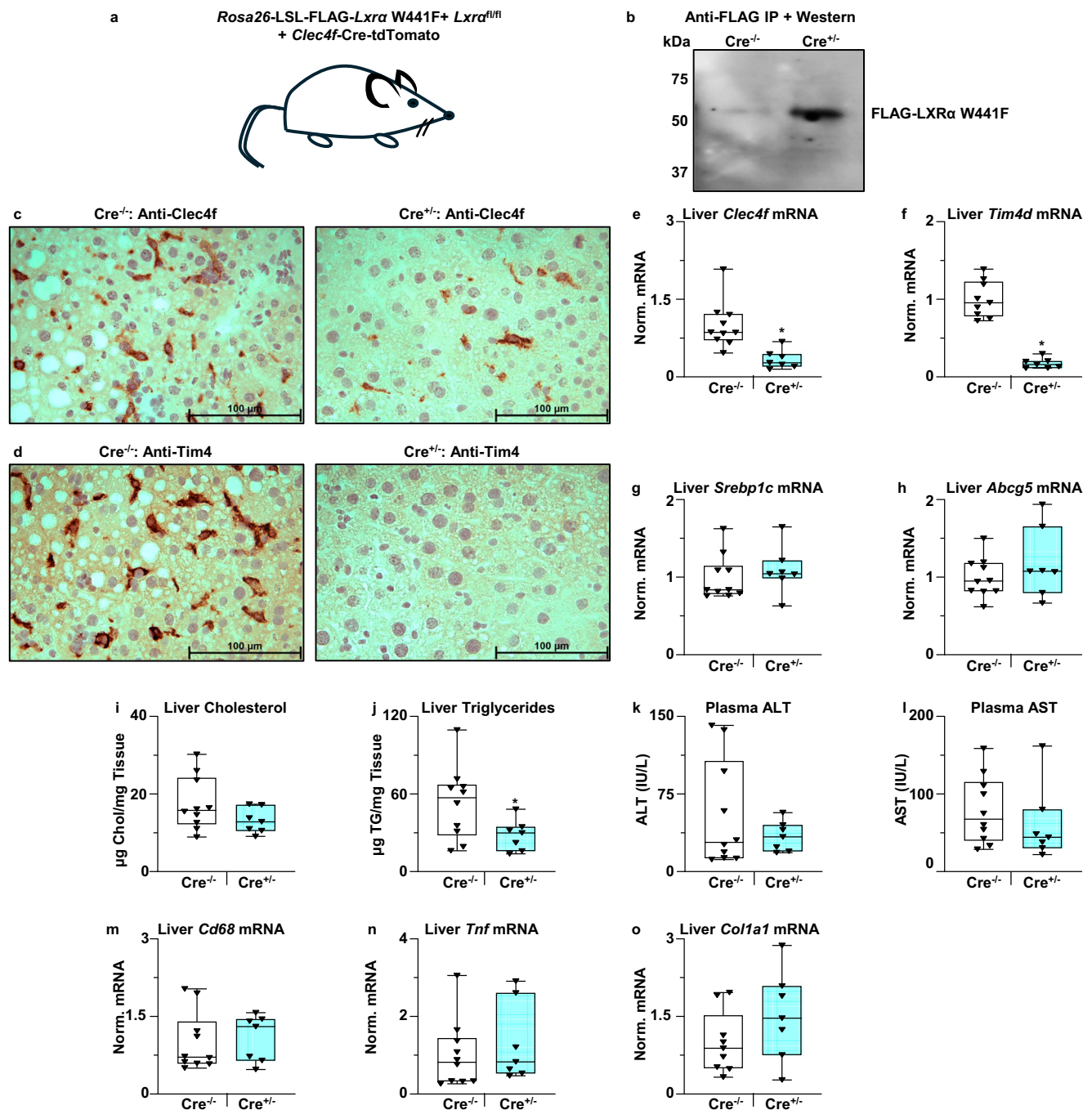


Fig. 10 | Kupffer cell-selective expression of LXRA W441F. Male 11–12 week old *Rosa26-LSL-FLAG-LXRα W441F/Lxrα^{fl/fl} + Clec4f-Cre-tdTomato* mice were fed the MASH diet for 4 weeks. **a** Experimental schematic. **b** Whole cell extracts were prepared from liver macrophage isolated from *Cre^{-/-}* and *Cre^{+/-}* mice, FLAG-tagged proteins were immune-purified and examined by Western blotting with anti-FLAG antibodies as described in the Methods. **c, d** Representative liver sections stained with antibodies recognizing Clec4f and Tim4. **e–h** Liver gene expression measured by real-time PCR as described in the Methods section. **i, j** Liver triglycerides and

cholesterol were measured as described in the methods section. **k, l** Plasma ALT and AST measured as described in the Methods section. **m–o** Liver gene expression measured by real-time PCR as described in the Methods section. *Statistically significant difference between *Cre^{-/-}* ($n = 10$) and *Cre^{+/-}* ($n = 7$) mice determined by two-tailed Mann–Whitney tests ($p \leq 0.05$). Boxes extend from the 25th–75th percentiles. The center line in the middle of the boxes represents the median. Whiskers extend from the lowest to the highest point. Source data are provided as Source Data file.

and pharmacological data is the observation that nuclear receptor antagonists often manifest tissue-specific and/or gene-selective agonist activity in vivo. The estrogen receptor ligand tamoxifen is a classic example of this phenomenon⁷². Finally, treatment of W441F mice with T0901317 reduces MASH by raising LXR activity from a low base to a level roughly equivalent to vehicle-treated control mice. Therefore, our data does not support treating MASH patients who have normal

LXR activity with synthetic agonists such as T0901317 to reach supra-physiological levels of activity that promote fatty liver and the secretion of VLDL.

Studies of MASH in mouse models have described an influx of Cx3cr1-expressing myeloid cells that give rise to lipid-associated macrophages expressing high levels of Trem2 and Gpnmb^{57–59}. Similar populations of lipid associated macrophages have been detected in

models of other chronic diseases associated with high cholesterol levels including atherosclerosis, diabetes, and Alzheimer's disease^{73–75}. The functions of lipid-associated macrophages and if they have beneficial or detrimental effects in different pathological settings is an area of active inquiry. In MASH there is also a loss of tissue resident macrophages (Kupffer cells) that are replaced by monocyte-derived cells^{60–63}. Similar increases in lipid-associated macrophages and decreases in Kupffer cell markers are detected in W441F mice. The decrease in Kupffer cells detected in W441F mice is consistent with the known role for LXR α as a lineage-determining factor for these cells^{59–62}. Strikingly, the macrophage landscape in W441F mice reverts to the control condition after reactivating LXR signaling. It will be interesting to identify the LXR-generated signals that revert the macrophage population in MASH and to see if these signals can be generated at other locations associated with altered myeloid populations including obese adipose tissue, atherosclerotic blood vessels and sites of amyloid beta deposition in Alzheimer's disease.

Selectively expressing W441F in hepatocytes recapitulates the MASH phenotypes detected when the mutant protein is expressed from the endogenous locus except for the loss of Kupffer cells. In contrast, selectively expressing W441F in Kupffer cells does not lead to MASH at least at the 4-week time point examined in this study. Lipid accumulation in hepatocytes is thought to be the initial insult in the development of MASH^{2,3,69}. Our results suggest that the accumulation of hepatic cholesterol may be at least one critical trigger that drives subsequent inflammation and fibrosis. The cholesterol-dependent phenotype seen in W441F mice is also consistent with studies in humans which correlate hepatic cholesterol levels with MASH^{5,6,8}. Cholesterol-dependent stabilization of the transcriptional cofactor TAZ in hepatocytes has been reported to contribute to the development of inflammation and fibrosis⁶⁷. Increased levels of TAZ protein are detected in the livers of male W441F mice after MASH diet feeding. Female W441F mice, however, have TAZ protein levels that are similar to controls. Taken together our results suggest that there may be TAZ-independent pathways that promote MASH in response to high cholesterol levels.

Heterozygous W441F mice provide a unique example of the interplay between the environment in the form of diet and genotype. On a normal chow diet, W/F mice exhibit decreased expression of LXR target genes, and consequently lower plasma lipid levels but otherwise appear normal. After 2 weeks of exposure to a MASH diet, however, these animals exhibit hepatic cholesterol accumulation, liver damage, inflammation, and fibrosis. There is also a corresponding change in the expression of over 4000 genes. Reactivation of LXR signaling in W/F mice reverses the effect of diet. Notably, the liver transcriptome in reactivated W/F mice closely resembles the transcriptome of vehicle-treated control mice which are steatotic but show no evidence of MASH. Going forward, we suggest that W/F mice provide a unique model system for identifying the factors that promote the development of MASH and for identifying potential therapeutic targets downstream of LXR signaling useful for reversing the disease.

Methods

The University of Virginia Animal care and Use Committee approved all animal experiments. The use of Biosafety level 2 reagents was approved by the University of Virginia Institutional Biosafety Committee.

Materials

Commercial reagents, chemicals, antibodies, mouse lines, cell lines, viruses, plasmids, and software used are listed in Supplemental Table 1. Sequence of the gRNA used to generate W441F mice and oligonucleotide sequences used for real-time PCR can be found in Supplemental Table 2.

In vitro experiments

Immortalized bone marrow derived macrophage (BMDM) isolated from *Lxra*^{-/-} + *Lxrb*^{-/-} mice⁴⁴ (a gift from P. Tontonoz) were cultured in BMDM media (DMEM + 20% FBS + 30% L929 conditioned media) and infected with adenovirus expressing GFP, FLAG-LXR α or FLAG-LXR α W441F at a ratio of 100 infectious viral particles/cell for 24 h. Following infection, cells were washed with phosphate buffered saline (PBS) and cultured for an additional 24 h in BMDM media in the presence or absence of 10 μ M 24,25-epoxycholesterol, 1.0 μ M T0901317, 1.0 μ M GW3965, or 1.0 μ M BMS852927. After ligand treatment, RNA was isolated using Quick-RNA miniprep kits, and mRNAs were quantified by real-time PCR. To examine the dominant negative activity of LXR α W441F, mouse AML12 cells cultured as recommended by the American Type Culture Collection (CRL-2254) were infected as described above. The media was changed 24 h post infection and RNA was isolated using Quick-RNA miniprep kits after an additional 24 h. Real-time PCR was used to quantify mRNA levels. For Western blotting, 30 μ g of nuclear extracts prepared as described by Liebergall et al.⁴¹ were resolved on 10% SDS polyacrylamide gels, transferred to Immobilon-P membranes, probed with antibodies to FLAG, LXR α or TBP and visualized with the appropriate alkaline phosphatase conjugated second antibodies.

Mice and in vivo experiments

The University of Virginia Animal care and Use Committee approved all animal experiments. CRISPR was used to replace tryptophan 441 at the *Nr1h3* locus with phenylalanine. Fertilized eggs from BgSJLF1/J mice were injected with Cas9 protein, a gRNA targeting the region around tryptophan 441 and a 200 nucleotide replacement sequence that changes the TGG tryptophan codon at amino acid 441 to TTC encoding phenylalanine. This change also creates a novel TCGA sequence that is a site for cleavage by the restriction enzyme TaqI-v2. Founders were identified by a combination of restriction enzyme digestion and DNA sequencing. The W441F allele was then backcrossed 6 times into C57BL/6J. All experiments used offspring of heterozygous crosses. Mice were fed Teklad LM-485 mouse/rat diet (normal chow) ad libitum on a 12 light/dark cycle at -21 °C. For experiments using the MASH diet, 11–12 week-old male and female mice were fed Teklad Custom Diet TD.96121 ad libitum for 4 weeks. After 2 weeks mice were dosed daily by oral gavage with vehicle (80% polyethylene glycol 400/20% Tween 80) or with 10 mg/kg T0901317 for an additional 2 weeks. Mice were bled via the retro-orbital sinus and tissues were isolated ~3 h after dosing. Body fat composition was measured using an EchoMRI™ Whole Body Composition Analyzer (version 150521).

To generate hepatocyte-selective W441F mice, a cDNA encoding mouse LXR α W441F with a 7 amino acid FLAG tag at the amino terminus was cloned into the *Rosa26* targeting vector pR26 CAG AsiSI/MluI (a gift from Ralf Kuehn) downstream of a Lox-Stop-Lox cassette. Cas9 protein, the donor plasmid, and a gRNA targeting *Rosa26* described by Chu et al.⁷⁶ were injected into fertilized eggs from BgSJLF1/J mice. Founders were identified by PCR and backcrossed 6 times with C57BL/6J mice. The final backcross utilized *Lxra*^{fl/fl} mice, in the C57BL/6J background, that have previously been described²³. The offspring of the last backcross were bred to each other to produce *Rosa26*-LSL-FLAG-LXR α W441F + *Lxra*^{fl/fl} mice. To examine the response to the MASH diet, 9–10 week-old female mice were injected via the tail vein with AAV-TBG-GFP or AAV-TBG-Cre (2 \times 10¹¹ viral genomes/mouse, gifts from James M. Wilson). After infection mice were maintained on a normal chow diet for 2 weeks before being switched to the MASH diet for 4 weeks. To generate Kupffer cell selective W441F mice, *Rosa26*-LSL-FLAG-LXR α W441F + *Lxra*^{fl/fl} mice were crossed with *Clec4f*-Cre-dtTomato mice⁶¹. To examine the response to the MASH diet, 11–12 old male Cre^{+/-} and Cre^{-/-} were fed the MASH diet for 4 weeks.

Plasma, hepatic, and fecal lipid measurements

Plasma total cholesterol, free cholesterol, triglycerides, glucose, ALT, and AST were measured using colorimetric assays listed in Supplemental Table 1 that were modified for use in 96 well plates. Hepatic lipids were extracted from ~50 mg of frozen samples as described by Breevoort et al.³¹. Dried extracts were resuspended in isopropanol: Triton X 100 (9:1). Cholesterol and triglycerides were measured using the colorimetric assays described in Supplemental Table 1 and normalized to the amount of starting tissue. To measure fecal bile acids, mice were housed individually for 48 h and feces from each animal were collected. Approximately 200 mg of feces was extracted as described by Breevoort et al.³¹ and bile acids were measured using the colorimetric assay. Bile acids were normalized by the milligram amount of feces.

Histochemistry and immunostaining

Antibodies and other reagents for histochemical staining are described in Supplemental Table 1. Freshly harvested liver tissues were fixed in 4% formaldehyde for 48 h and embedded in paraffin. For staining, 10 micron thick sections were deparaffinized, and stained with H&E or with Picrosirius Red (0.1% Direct Red 80 in a saturated aqueous solution of picric acid). Images were captured using the Leica Application Suite X 3.7.6.25997. To quantify collagen staining, ImagePro Plus was used to determine the percentage of Picrosirius Red positive area in 5 independent sections/mouse. For Oil Red O staining, freshly harvested liver and spleen samples were frozen in OTC and 10 micron thick sections were fixed in 60% ethanol for 10 min, stained with 0.21% Oil Red O in 60% isopropanol for 20 min, washed with water and then stained for 3 min with Hematoxylin QS. For immunostaining of Cd68, Clec4f, and Ki67, 10 micron thick frozen sections were fixed in 95% ethanol for 30 min and treated with BLOXALL for 10 min to inhibit endogenous peroxidase activity. Sections were then treated with Avidin and Biotin blocking solutions before incubation with primary antibodies for 1 h followed by biotinylated second antibodies for 30 min. Staining was visualized using Avidin-Biotin Complex reagent followed by NovaRed staining. Nuclei were counter stained with Hematoxylin QS for 3 min.

Liver extracts and Western blotting

To prepare nuclear extracts ~50 mg of frozen liver in Lysing Matrix D tubes with 1.0 ml of Buffer A (10 mM HEPES pH 7.9, 10 mM KCl, 0.1 mM EDTA, 0.1 mM EGTA, 1.0 mM DTT, 0.6% NP-40, 1.0 mM PMSF, 25 µg/ml Aprotinin, 5 µg/ml Leupeptin, 1 µg/ml Pepstatin) were disrupted by sequential 30 s bursts in a FASTPREP 24 machine (MP Biochemicals) at speed setting 6 until a homogenous suspension was apparent. The suspension was then incubated on ice for an additional 5 min. Nuclei were pelleted for 1 min at 16,000 × *g* at 4 °C, the pellet was resuspended in 200 µl of Buffer A, pelleted as before, and extracted in 50 µl of Buffer C (10 mM HEPES pH 7.9, 400 nM NaCl, 1.0 mM EDTA, 1.0 mM EGTA, 1.0 mM DTT, 0.6% NP-40, 1.0 mM PMSF, 25 µg/ml Aprotinin, 5 µg/ml Leupeptin, 1 µg/ml Pepstatin) for 15 min at 4 °C with moderate shaking. Samples were pelleted for 5 min at 16,000 × *g* at 4 °C, supernatants were collected, and protein amounts were quantified by BCA assays. For Western blotting, 30 µg of nuclear extract was resolved on 10% SDS polyacrylamide gels, transferred to Immobilon-P membranes, probed with antibodies to FLAG, LXRα or TBP and visualized with the appropriate alkaline phosphatase-conjugated second antibodies. For whole cell extracts approximately 50 mg of frozen liver in Lysing Matrix D tubes with 0.5 ml of RIPA buffer (10 mM Tris pH 8.0, 1.0 mM EDTA, 1.0 mM EGTA, 0.1% SDS, 0.1% deoxycholate, 1.0% Triton X-100/1.0 mM PMSF, 25 µg/ml Aprotinin, 5 µg/ml Leupeptin, 1 µg/ml Pepstatin) was disrupted in a FASTPREP 24 Machine (MP Biochemicals) as described above. Extracts were incubated on ice for 5 min, pelleted for 10 min at 16,000 × *g* at 4 °C, supernatants were collected, sheared with

a 1cc Insulin syringe, and pelleted for 5 min at 16,000 × *g* at 4 °C. Supernatants were collected and protein amounts were quantified by BCA assays. Western blotting was carried out as described above using antibodies recognizing TAZ and GAPDH.

Liver macrophage isolation and FLAG-LXRα W441F purification

Enriched populations of liver macrophages were isolated as described by Li et al.⁷⁷. Following isolation, red blood cells were lysed and the remaining cells were plated in 6 cm plates in 2.0 ml of RPMI media containing 10% fetal bovine serum and incubated at 37 °C in 5% CO₂ for 30 min. Cells were washed extensively with PBS and RNA was isolated using Quick-RNA miniprep kits. To examine protein levels of FLAG-LXRα W441F in liver macrophages, cells isolated as described above from 3 Cre^{-/-} or 3 Cre^{+/-} mice were pooled, lysed in 500 µl of RIPA buffer and ~400 µg of total protein was incubated with constant inversion for 4 h at 4 °C with 20 µl of magnetic anti-FLAG beads. The beads were washed 3 times with 500 µl of RIPA buffer, once with 500 µl of PBS, and protein was eluted from the beads by incubating for 15 min at 4 °C with constant inversion in PBS containing 50 ng of 3x FLAG peptide. FLAG-LXRα W441F protein levels were examined by Western blotting using anti-FLAG antibodies.

RNA Isolation from mouse tissues, real-time PCR, and RNA-Seq

Approximately 25 mg of tissue in Lysing Matrix D tubes with 0.5 ml of Triazole were disrupted for 30 s bursts in a FASTPREP 24 machine (MP Biochemicals) at speed setting 3. Following extraction with chloroform, total RNA was isolated from the aqueous layer using Quick-RNA miniprep kits. DNase treatment, reverse transcription and real-time PCR were conducted as described by Liebergall et al.⁴¹ using a BIO-RAD CSF Connect system. Primers are listed in Supplemental Table 2. RNA-Seq using poly-A selected liver RNA isolated from male mice was conducted by Azenta Life Sciences. For each sample, at least 20 million sequence reads were obtained. Sequence reads were trimmed to remove possible adapter sequences and nucleotides with poor quality using Trimmomatic v.0.36. The trimmed reads were mapped to the *Mus musculus* GRCm38 reference genome available on ENSEMBL using the STAR aligner v.2.5.2b. Unique gene hit counts were calculated by using featureCounts from the Subread package v.1.5.2. Only unique reads that fell within exon regions were counted. After extraction of gene hit counts, the gene hit counts table was used for downstream differential expression analysis. Using DESeq2, a comparison of gene expression between defined groups of samples was performed. The Wald test was used to generate *p*-values and log₂ fold changes. Genes with an adjusted *p*-value < 0.05 and absolute log₂ fold change >1 were called as differentially expressed genes for each comparison.

Statistical and reproducibility

All analysis was conducted using GraphPad Prism. Data sets were first tested for normal distributions. Experiments with normal distributions were examined using 1-way ANOVA, two-way ANOVA, or unpaired two-tailed *t*-tests. Two-tailed Mann-Whitney tests were used to data sets that did not meet a normal distribution. Micrographs of H&E, Oil Red O, and immunohistochemically stained liver sections are representative images from 4 independent sections/mouse, 5 mice/group for a total of 20 stained sections/group. Micrographs of Picrosirius Red stained liver sections are representative images from 10 independent sections/mouse, 5 mice/group for a total of 50 stained sections/group. Western blots were repeated at least 2 times.

Reporting summary

Further information on research design is available in the Nature Portfolio Reporting Summary linked to this article.

Data availability

The authors declare that the data supporting the findings of this study are available within the paper and its supplementary information file. Source data are provided with this paper. Reagents and mouse lines are available upon request from the corresponding author. RNA sequencing data are available at the Gene Expression Omnibus accession number [GSE267011](https://www.ncbi.nlm.nih.gov/geo/query/acc.cgi?acc=GSE267011). Source data are provided with this paper.

References

- Hamid, O. et al. The epidemiology of non-alcoholic steatohepatitis (NASH) in the United States between 2010–2020: a population-based study. *Ann. Hepatol.* **27**, 100727 (2022).
- Schwabe, R. F., Tabas, I. & Pajvani, U. B. Mechanisms of fibrosis development in nonalcoholic steatohepatitis. *Gastroenterology* **158**, 1913–1928 (2020).
- Engin, A. Non-alcoholic fatty liver disease. *Adv. Exp. Med. Biol.* **960**, 443–467 (2017).
- Jensen, T. et al. Fructose and sugar: a major mediator of non-alcoholic fatty liver disease. *J. Hepatol.* **68**, 1063–1075 (2018).
- Caballero, F. et al. Enhanced free cholesterol, SREBP-2 and StAR expression in human NASH. *J. Hepatol.* **50**, 789–796 (2009).
- Ioannou, G. N. The role of cholesterol in the pathogenesis of NASH. *Trends Endocrinol. Metab.* **27**, 84–95 (2016).
- Min, H. K. et al. Increased hepatic synthesis and dysregulation of cholesterol metabolism is associated with the severity of nonalcoholic fatty liver disease. *Cell Metab.* **15**, 665–674 (2012).
- Puri, P. et al. A lipidomic analysis of nonalcoholic fatty liver disease. *Hepatology* **46**, 1081–1090 (2007).
- Athyros, V. G. et al. The use of statins alone, or in combination with pioglitazone and other drugs, for the treatment of non-alcoholic fatty liver disease/non-alcoholic steatohepatitis and related cardiovascular risk. An Expert Panel Statement. *Metabolism* **71**, 17–32 (2017).
- Athyros, V. G. et al. Statins: an under-appreciated asset for the prevention and the treatment of NAFLD or NASH and the related cardiovascular risk. *Curr. Vasc. Pharm.* **16**, 246–253 (2018).
- Doumas, M. et al. The role of statins in the management of non-alcoholic fatty liver disease. *Curr. Pharm. Des.* **24**, 4587–4592 (2018).
- Nascimbeni, F. et al. Statins and nonalcoholic fatty liver disease in the era of precision medicine: More friends than foes. *Atherosclerosis* **284**, 66–74 (2019).
- Sigler, M. A., Congdon, L. & Edwards, K. L. An evidence-based review of statin use in patients with nonalcoholic fatty liver disease. *Clin. Med Insights Gastroenterol.* **11**, 1179552218787502 (2018).
- McGettigan, B. et al. Dietary lipids differentially shape nonalcoholic steatohepatitis progression and the transcriptome of Kupffer cells and infiltrating macrophages. *Hepatology* **70**, 67–83 (2019).
- Savard, C. et al. Synergistic interaction of dietary cholesterol and dietary fat in inducing experimental steatohepatitis. *Hepatology* **57**, 81–92 (2013).
- Wouters, K. et al. Dietary cholesterol, rather than liver steatosis, leads to hepatic inflammation in hyperlipidemic mouse models of nonalcoholic steatohepatitis. *Hepatology* **48**, 474–486 (2008).
- Van Rooyen, D. M. et al. Hepatic free cholesterol accumulates in obese, diabetic mice and causes nonalcoholic steatohepatitis. *Gastroenterology* **141**, 1393–1403 (2011). 1403 e1391-1395.
- Hong, C. & Tontonoz, P. Liver X receptors in lipid metabolism: opportunities for drug discovery. *Nat. Rev. Drug Discov.* **13**, 433–444 (2014).
- Russo-Savage, L. & Schulman, I. G. Liver X receptors and liver physiology. *Biochim Biophys. Acta Mol. Basis Dis.* **1867**, 166121 (2021).
- Zelcer, N. & Tontonoz, P. Liver X receptors as integrators of metabolic and inflammatory signaling. *J. Clin. Invest.* **116**, 607–614 (2006).
- Schulman, I. G. Liver X receptors link lipid metabolism and inflammation. *FEBS Lett.* **591**, 2978–2991 (2017).
- Peet, D. J. et al. Cholesterol and bile acid metabolism are impaired in mice lacking the nuclear oxysterol receptor LXRα. *Cell* **93**, 693–704 (1998).
- Zhang, Y. et al. Liver LXRα expression is crucial for whole body cholesterol homeostasis and reverse cholesterol transport in mice. *J. Clin. Invest.* **122**, 1688–1699 (2012).
- Repa, J. J. et al. Regulation of ATP-binding cassette sterol transporters ABCG5 and ABCG8 by the liver X receptors α and β. *J. Biol. Chem.* **277**, 18793–18800 (2002).
- Repa, J. J. et al. Regulation of mouse sterol regulatory element-binding protein-1c gene (SREBP-1c) by oxysterol receptors, LXRα and LXRβ. *Genes Dev.* **14**, 2819–2830 (2000).
- Schultz, J. R. et al. Role of LXRs in control of lipogenesis. *Genes Dev.* **14**, 2831–2838 (2000).
- Griffett, K. & Burris, T. P. Development of LXR inverse agonists to treat MAFLD, NASH, and other metabolic diseases. *Front. Med.* **10**, 1102469 (2023).
- Griffett, K., Solt, L. A., El-Gendy, BelD., Kamenecka, T. M. & Burris, T. P. A liver-selective LXR inverse agonist that suppresses hepatic steatosis. *ACS Chem. Biol.* **8**, 559–567 (2013).
- Griffett, K. et al. The LXR inverse agonist SR9238 suppresses fibrosis in a model of non-alcoholic steatohepatitis. *Mol. Metab.* **4**, 353–357 (2015).
- Huang, P. et al. Liver X receptor inverse agonist SR9243 suppresses nonalcoholic steatohepatitis intrahepatic inflammation and fibrosis. *Biomed. Res. Int.* **2018**, 8071093 (2018).
- Breevoort, S. R., Angdisen, J. & Schulman, I. G. Macrophage-independent regulation of reverse cholesterol transport by liver X receptors. *Arterioscler Thromb. Vasc. Biol.* **34**, 1650–1660 (2014).
- Fowler, A. J. et al. Liver X receptor activators display anti-inflammatory activity in irritant and allergic contact dermatitis models: liver-X-receptor-specific inhibition of inflammation and primary cytokine production. *J. Invest. Dermatol.* **120**, 246–255 (2003).
- Cao, G. et al. Antidiabetic action of a liver x receptor agonist mediated by inhibition of hepatic gluconeogenesis. *J. Biol. Chem.* **278**, 1131–1136 (2003).
- Joseph, S. B. et al. Synthetic LXR ligand inhibits the development of atherosclerosis in mice. *Proc. Natl Acad. Sci. USA* **99**, 7604–7609 (2002).
- Tangirala, R. K. et al. Identification of macrophage liver X receptors as inhibitors of atherosclerosis. *Proc. Natl Acad. Sci. USA* **99**, 11896–11901 (2002).
- Terasaka, N. et al. T-0901317, a synthetic liver X receptor ligand, inhibits development of atherosclerosis in LDL receptor-deficient mice. *FEBS Lett.* **536**, 6–11 (2003).
- Hoffmann, T. J. et al. A large electronic-health-record-based genome-wide study of serum lipids. *Nat. Genet.* **50**, 401–413 (2018).
- Klarin, D. et al. Genetics of blood lipids among ~300,000 multi-ethnic participants of the Million Veteran Program. *Nat. Genet.* **50**, 1514–1523 (2018).
- Cornes, B. K. et al. Association of levels of fasting glucose and insulin with rare variants at the chromosome 11p11.2-MADD locus: cohorts for Heart and Aging Research in Genomic Epidemiology (CHARGE) Consortium Targeted Sequencing Study. *Circ. Cardiovasc. Genet.* **7**, 374–382 (2014).
- Lockhart, S. M. et al. Damaging mutations in liver X receptor-α are hepatotoxic and implicate cholesterol sensing in liver health. *Nat. Metab.* **6**, 1922–1938 (2024).

41. Liebergall, S. R. et al. Inflammation triggers liver X receptor-dependent lipogenesis. *Mol. Cell Biol.* **40**, 1–21 (2020).
42. Svensson, S. et al. Crystal structure of the heterodimeric complex of LXRA and RXR β ligand-binding domains in a fully agonistic conformation. *EMBO J.* **22**, 4625–4633 (2003).
43. Williams, S. et al. X-ray crystal structure of the liver X receptor beta ligand binding domain: regulation by a histidine-tryptophan switch. *J. Biol. Chem.* **278**, 27138–27143 (2003).
44. Ito, A. et al. LXRs link metabolism to inflammation through Abca1-dependent regulation of membrane composition and TLR signaling. *eLife* **4**, e08009 (2015).
45. Farnegardh, M. et al. The three-dimensional structure of the liver X receptor beta reveals a flexible ligand-binding pocket that can accommodate fundamentally different ligands. *J. Biol. Chem.* **278**, 38821–38828 (2003).
46. Fradera, X. et al. X-ray structures of the LXRA LBD in its homodimeric form and implications for heterodimer signaling. *J. Mol. Biol.* **399**, 120–132 (2010).
47. Kick, E. K. et al. Discovery of highly potent liver X receptor beta agonists. *ACS Med. Chem. Lett.* **7**, 1207–1212 (2016).
48. Ignatova, I. D., Angdisen, J., Moran, E. & Schulman, I. G. Differential regulation of gene expression by LXRs in response to macrophage cholesterol loading. *Mol. Endocrinol.* **27**, 1036–1047 (2013).
49. Basciano, H., Miller, A., Baker, C., Naples, M. & Adeli, K. LXRA activation perturbs hepatic insulin signaling and stimulates production of apolipoprotein B-containing lipoproteins. *Am. J. Physiol. Gastrointest. Liver Physiol.* **297**, G323–G332 (2009).
50. Grefhorst, A. et al. Stimulation of lipogenesis by pharmacological activation of the liver X receptor leads to production of large, triglyceride-rich very low density lipoprotein particles. *J. Biol. Chem.* **277**, 34182–34190 (2002).
51. Brunham, L. R. et al. Tissue-specific induction of intestinal ABCA1 expression with a liver X receptor agonist raises plasma HDL cholesterol levels. *Circ. Res.* **99**, 672–674 (2006).
52. Repa, J. J. et al. Regulation of absorption and ABC1-mediated efflux of cholesterol by RXR heterodimers. *Science* **289**, 1524–1529 (2000).
53. Bensinger, S. J. et al. LXR signaling couples sterol metabolism to proliferation in the acquired immune response. *Cell* **134**, 97–111 (2008).
54. Murphy, A. J. et al. ApoE regulates hematopoietic stem cell proliferation, monocytoysis, and monocyte accumulation in atherosclerotic lesions in mice. *J. Clin. Invest.* **121**, 4138–4149 (2011).
55. Wang, B. et al. Phospholipid remodeling and cholesterol availability regulate intestinal stemness and tumorigenesis. *Cell Stem Cell* **22**, 206–220 e204 (2018).
56. Boergesen, M. et al. Genome-wide profiling of liver X receptor, retinoid X receptor, and peroxisome proliferator-activated receptor alpha in mouse liver reveals extensive sharing of binding sites. *Mol. Cell Biol.* **32**, 852–867 (2012).
57. Daemen, S. et al. Dynamic shifts in the composition of resident and recruited macrophages influence tissue remodeling in NASH. *Cell Rep.* **34**, 108626 (2021).
58. Remmerie, A. et al. Osteopontin expression identifies a subset of recruited macrophages distinct from Kupffer cells in the fatty liver. *Immunity* **53**, 641–657.e614 (2020).
59. Seidman, J. S. et al. Niche-specific reprogramming of epigenetic landscapes drives myeloid cell diversity in nonalcoholic steatohepatitis. *Immunity* **52**, 1057–1074.e1057 (2020).
60. Bonnardel, J. et al. Stellate cells, hepatocytes, and endothelial cells imprint the Kupffer cell identity on monocytes colonizing the liver macrophage niche. *Immunity* **51**, 638–654.e639 (2019).
61. Sakai, M. et al. Liver-derived signals sequentially reprogram myeloid enhancers to initiate and maintain Kupffer cell identity. *Immunity* **51**, 655–670.e658 (2019).
62. Scott, C. L. et al. The transcription factor ZEB2 is required to maintain the tissue-specific identities of macrophages. *Immunity* **49**, 312–325.e315 (2018).
63. Tran, S. et al. Impaired Kupffer cell self-renewal alters the liver response to lipid overload during non-alcoholic steatohepatitis. *Immunity* **53**, 627–640.e625 (2020).
64. Khajehahmadi, Z. et al. Downregulation of hedgehog ligands in human simple steatosis may protect against nonalcoholic steatohepatitis: is TAZ a crucial regulator? *IUBMB Life* **71**, 1382–1390 (2019).
65. Mooring, M. et al. Hepatocyte stress increases expression of yes-associated protein and transcriptional coactivator with PDZ-binding motif in hepatocytes to promote parenchymal inflammation and fibrosis. *Hepatology* **71**, 1813–1830 (2020).
66. Wang, X. et al. Hepatocyte TAZ/WWTR1 promotes inflammation and fibrosis in nonalcoholic steatohepatitis. *Cell Metab.* **24**, 848–862 (2016).
67. Wang, X. et al. Cholesterol stabilizes TAZ in hepatocytes to promote experimental non-alcoholic steatohepatitis. *Cell Metab.* **31**, 969–986.e967 (2020).
68. Wang, X. et al. A therapeutic silencing RNA targeting hepatocyte TAZ prevents and reverses fibrosis in nonalcoholic steatohepatitis in mice. *Hepatol. Commun.* **3**, 1221–1234 (2019).
69. Sheka, A. C. et al. Nonalcoholic steatohepatitis: a review. *JAMA* **323**, 1175–1183 (2020).
70. Ghisletti, S. et al. Cooperative NCoR/SMRT interactions establish a corepressor-based strategy for integration of inflammatory and anti-inflammatory signaling pathways. *Genes Dev.* **23**, 681–693 (2009).
71. Oishi, Y. et al. SREBP1 contributes to resolution of pro-inflammatory TLR4 signaling by reprogramming fatty acid metabolism. *Cell Metab.* **25**, 412–427 (2017).
72. McDonnell, D. P. & Wardell, S. E. The molecular mechanisms underlying the pharmacological actions of ER modulators: implications for new drug discovery in breast cancer. *Curr. Opin. Pharm.* **10**, 620–628 (2010).
73. Deczkowska, A. et al. Disease-associated microglia: a universal immune sensor of neurodegeneration. *Cell* **173**, 1073–1081 (2018).
74. Kim, K., Park, S. E., Park, J. S. & Choi, J. H. Characteristics of plaque lipid-associated macrophages and their possible roles in the pathogenesis of atherosclerosis. *Curr. Opin. Lipidol.* **33**, 283–288 (2022).
75. Jaitin, D. A. et al. Lipid-associated macrophages control metabolic homeostasis in a Trem2-dependent manner. *Cell* **178**, 686–698.e614 (2019).
76. Chu, V. T. et al. Efficient generation of Rosa26 knock-in mice using CRISPR/Cas9 in C57BL/6 zygotes. *BMC Biotechnol.* **16**, 4 (2016).
77. Li, P. Z., Li, J. Z., Li, M., Gong, J. P. & He, K. An efficient method to isolate and culture mouse Kupffer cells. *Immunol. Lett.* **158**, 52–56 (2014).

Acknowledgements

This work was supported by grants from the NIH/NIDDK (1R01DK130050-01A1) and NIH/NIA (1R21AG075577-01A1) to I.G.S. Micrographs were obtained using the Leica Thunder Microscope in the University of Virginia Advanced Microscopy Facility. Mouse lines were made by the University of Virginia Genetically Engineered Mouse Model Core. Tissue sectioning and H&E staining were provided by the University of Virginia Research Histology Core. All core facilities are supported by the University of Virginia School of Medicine, and through the University of Virginia Cancer Center National Cancer Institute P30 Center Grant.

Author contributions

A.T.C., L.R.-S., and I.G.S. designed experiments, performed experiments, and interpreted data. I.G.S. wrote the manuscript. L.A.A. and N.H. genotyped mice and performed histological staining. N.A.A. measured tissue and plasma lipids.

Competing interests

The authors declare no competing interests.

Additional information

Supplementary information The online version contains supplementary material available at <https://doi.org/10.1038/s41467-025-56565-8>.

Correspondence and requests for materials should be addressed to Ira G. Schulman.

Peer review information *Nature Communications* thanks the anonymous, reviewer(s) for their contribution to the peer review of this work. A peer review file is available.

Reprints and permissions information is available at <http://www.nature.com/reprints>

Publisher's note Springer Nature remains neutral with regard to jurisdictional claims in published maps and institutional affiliations.

Open Access This article is licensed under a Creative Commons Attribution-NonCommercial-NoDerivatives 4.0 International License, which permits any non-commercial use, sharing, distribution and reproduction in any medium or format, as long as you give appropriate credit to the original author(s) and the source, provide a link to the Creative Commons licence, and indicate if you modified the licensed material. You do not have permission under this licence to share adapted material derived from this article or parts of it. The images or other third party material in this article are included in the article's Creative Commons licence, unless indicated otherwise in a credit line to the material. If material is not included in the article's Creative Commons licence and your intended use is not permitted by statutory regulation or exceeds the permitted use, you will need to obtain permission directly from the copyright holder. To view a copy of this licence, visit <http://creativecommons.org/licenses/by-nc-nd/4.0/>.

© The Author(s) 2025